



CMS-SMP-20-005

CERN-EP-2021-219
2022/03/11

Measurement of $W^\pm\gamma$ differential cross sections in proton-proton collisions at $\sqrt{s} = 13$ TeV and effective field theory constraints

The CMS Collaboration^{*}

Abstract

Differential cross section measurements of $W^\pm\gamma$ production in proton-proton collisions at $\sqrt{s} = 13$ TeV are presented. The data set used in this study was collected with the CMS detector at the CERN LHC in 2016–2018 with an integrated luminosity of 138 fb^{-1} . Candidate events containing an electron or muon, a photon, and missing transverse momentum are selected. The measurements are compared with standard model predictions computed at next-to-leading and next-to-next-to-leading orders in perturbative quantum chromodynamics. Constraints on the presence of TeV-scale new physics affecting the $WW\gamma$ vertex are determined within an effective field theory framework, focusing on the \mathcal{O}_{3W} operator. A simultaneous measurement of the photon transverse momentum and the azimuthal angle of the charged lepton in a special reference frame is performed. This two-dimensional approach provides up to a factor of ten more sensitivity to the interference between the standard model and the \mathcal{O}_{3W} contribution than using the transverse momentum alone.

Published in Physical Review D as doi:10.1103/PhysRevD.105.052003.

1 Introduction

The measurement of the properties of vector boson pair production is an important test of the electroweak sector of the standard model (SM). The production cross sections of these processes are sensitive to the WWV triple gauge couplings (TGCs), where $V = \gamma$ or Z . Because the strengths of these TGCs are predicted precisely in the SM, the measurement of an anomalous value would indicate the presence of physics beyond the SM (BSM).

This paper reports an analysis of $W^\pm\gamma$ production in proton-proton (pp) collisions at $\sqrt{s} = 13$ TeV using data recorded with the CMS detector at the CERN LHC in 2016–2018 with an integrated luminosity of 138 fb^{-1} . This process has previously been studied by the CDF and D0 Collaborations [1–3] at the Fermilab Tevatron in $p\bar{p}$ collisions at $\sqrt{s} = 1.96$ TeV, and by the CMS [4] and ATLAS [5] Collaborations using pp collision data collected at $\sqrt{s} = 7$ TeV. The CMS Collaboration has also performed the first $W^\pm\gamma$ measurement at $\sqrt{s} = 13$ TeV [6]. All of these studies found the measured inclusive cross sections to be compatible with the SM predictions and set limits on the presence of anomalous TGCs.

In the present analysis, $W^\pm\gamma$ events are selected with one charged lepton (ℓ), which is either an electron or muon, one neutrino (ν), and one photon (γ) in the final state. A few leading order (LO) Feynman diagrams are shown in Fig. 1. The photon can be produced as a result of either initial- or final-state radiation, in addition to the contribution involving a TGC vertex.

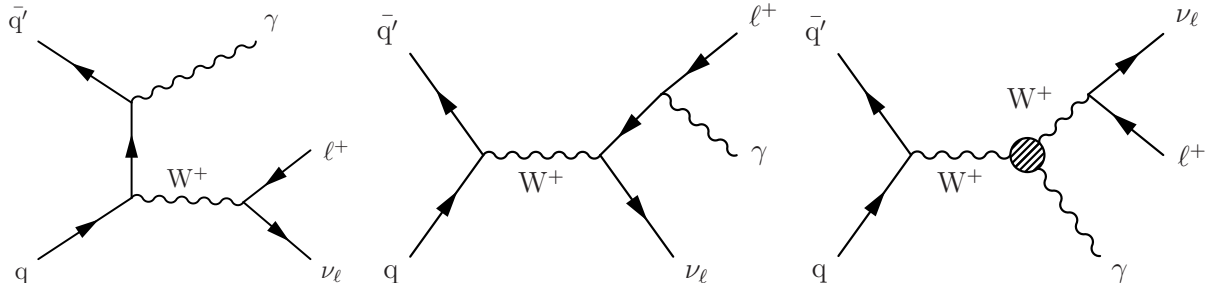


Figure 1: LO Feynman diagrams for $W^+\gamma$ production showing initial-state (left) and final-state (center) radiation of the photon, and the $WW\gamma$ TGC process (right).

Differential cross sections are measured for several observables, including the transverse momentum p_T^γ and pseudorapidity η^γ of the photon, and the transverse mass of the $\ell\nu\gamma$ system, denoted m_T^{cluster} . The cross section is also measured as a function of the number of additional jets. The measured values are compared with the SM predictions at next-to-leading order (NLO) and next-to-next-to-leading order (NNLO) in perturbative quantum chromodynamics (QCD). Interference between the LO $W^\pm\gamma$ production diagrams results in a cross section that vanishes in specific phase space regions. This effect is known as a radiation amplitude zero (RAZ) [7–11]. A differential cross section measurement of the pseudorapidity difference between the lepton and the photon, $\Delta\eta(\ell, \gamma)$, is used to explore this effect.

Constraints on BSM contributions to the $WW\gamma$ vertex are determined in an effective field theory (EFT) framework. For the first time in the study of this process, both p_T^γ and the angular properties of the final-state particles are exploited to increase the sensitivity to the interference between the SM and BSM amplitudes. This novel approach is referred to as “interference resurrection” [12, 13].

The paper is organized as follows. The interference resurrection technique is described in Section 2. The CMS detector, data samples, and event simulation are summarized in Sections 3 and 4. The object reconstruction and event selection are described in Sections 5 and 6. The

estimation of the main backgrounds is given in Section 7. The systematic uncertainties are discussed in Section 8, the results presented in Section 9, and the paper summarized in Section 10.

2 Interference resurrection

An EFT approach can be used to study how new physics entering at an energy scale Λ , assumed to be much larger than the electroweak scale, leads to deviations from the SM at an energy regime accessible at the LHC. The SM EFT is constructed by the addition of higher-dimensional operators, \mathcal{O}_i , to the SM Lagrangian,

$$\mathcal{L}_{\text{EFT}} = \mathcal{L}_{\text{SM}} + \sum_i C_i^{(6)} \mathcal{O}_i^{(6)} + \sum_i C_i^{(8)} \mathcal{O}_i^{(8)} + \dots, \quad (1)$$

where i enumerates the set of operators under consideration, $C_i^{(D)}$ are Wilson coefficients that scale as Λ^{4-D} and D denotes the operator dimension. The leading deviations from the SM are generally expected to occur at $D = 6$, since $D = 5$ operators violate lepton number conservation [14]. Examples of the relationship between the operators affecting diboson production and specific BSM scenarios are described in Refs. [15, 16].

The dimension-six operator of interest in this analysis, \mathcal{O}_{3W} , is a CP -even modification of the WWV TGC defined in the EFT basis of Ref. [17] as

$$\mathcal{O}_{3W} = \epsilon^{ijk} W_\mu^{i\nu} W_\nu^{j\rho} W_\rho^{k\mu}, \quad (2)$$

where $W_\mu^{i\nu}$ is the weak isospin field strength tensor and ϵ^{ijk} is the totally antisymmetric tensor with $\epsilon^{123} = 1$. The cross section in the presence of this operator can be expressed as

$$\sigma(C_{3W}) = \sigma^{\text{SM}} + C_{3W} \sigma^{\text{int}} + C_{3W}^2 \sigma^{\text{BSM}}, \quad (3)$$

where C_{3W} is the Wilson coefficient, σ^{int} is the contribution from the interference between the SM and \mathcal{O}_{3W} , and σ^{BSM} is the pure BSM component.

However, it has been demonstrated [12, 13] that in the high-energy limit, $E > m_W$, the $2 \rightarrow 2$ amplitudes for transverse vector boson production, $ff \rightarrow W_T V_T$, have different final-state helicity configurations for the SM ($\pm\mp$) and BSM ($\pm\pm$) components. This means the effect of the interference is typically not detectable when considering observables inclusive over the decay angles, for example, the p_T of the photon or W^\pm boson. This narrows our sensitivity in such observables to just the pure BSM contribution at order C_{3W}^2 , which scales as Λ^{-4} . In this scenario, the validity of any derived constraints can be limited by the unknown effect of the leading dimension-eight contributions, which also enter at order Λ^{-4} . Therefore, increasing the sensitivity to the interference, which scales as Λ^{-2} , is important for improving the validity of the constraints in any global EFT interpretation [18].

A method has been proposed [12, 19] that gives sensitivity to the SM-BSM interference by measuring the decay angles of the final-state fermions. A special coordinate system, illustrated in Fig. 2, is defined event-by-event by a Lorentz boost to the center-of-mass frame of the $W^\pm\gamma$ system, where the boost direction is denoted \hat{r} . Since the longitudinal component of the neutrino momentum is not measurable, additional constraints are required in the calculation of the $W^\pm\gamma$ four-momentum, described in Section 6.1. In the boosted frame the boson momenta are back-to-back, and the z axis is taken as the direction of the W^\pm boson, the y axis direction is given by $\hat{z} \times \hat{r}$, and the x axis given by $\hat{y} \times \hat{z}$. The final-state fermions from the W^\pm boson

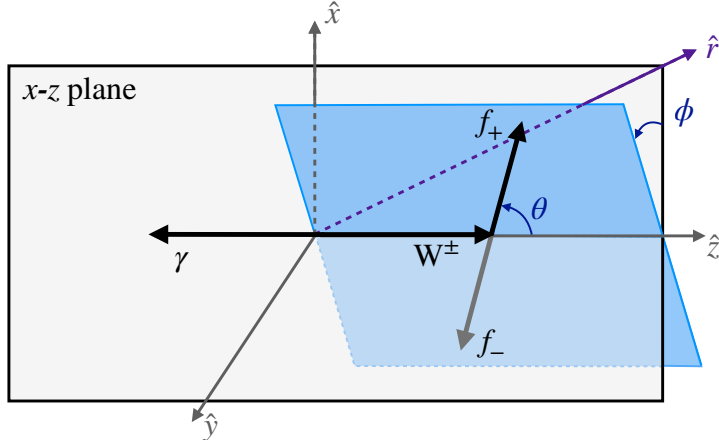


Figure 2: Scheme of the special coordinate system for $W^\pm\gamma$ production, defined by a Lorentz boost to the center-of-mass frame along the direction \hat{r} . The z axis is chosen as the W^\pm boson direction in this frame, and y is given by $\hat{z} \times \hat{r}$. The W^\pm boson decay plane is indicated in blue, where the labels f_+ and f_- refer to positive and negative helicity final-state fermions. The angles ϕ and θ are the azimuthal and polar angles of f_+ .

decay are labeled as f_+ and f_- , referring to the positive and negative fermion helicity states, respectively.

In this frame the angle θ is the polar angle of the W^\pm boson decay in its rest frame, taken as the angle between the three-momenta of the W^\pm boson and fermion f_+ . The angle $\phi \in [-\pi, \pi]$ is the azimuthal angle of f_+ : $\phi = \phi(f_+) = \phi(f_-) + \pi$, modulo 2π .

A measurement of ϕ is sensitive to the interference of the \mathcal{O}_{3W} term with the SM contribution. Figure 3 (left) shows the particle-level distribution in ϕ in the LO $2 \rightarrow 2$ scattering process for varying values of C_{3W} , with only the inclusion of the interference term. A clear modulation is present, which grows with increasing C_{3W} . Figure 3 (right) shows that the magnitude of this modulation is reduced with the inclusion of additional jets in the matrix element calculations, with MLM merging [20] used in the matching to the parton shower. However, a veto on the presence of additional jets in the event with $p_T > 30$ GeV and $|\eta| < 2.5$ is shown to substantially restore the effect.

3 The CMS detector

The central feature of the CMS apparatus is a superconducting solenoid of 6 m internal diameter, providing a magnetic field of 3.8 T. Within the solenoid volume are a silicon pixel and strip tracker, a lead tungstate crystal electromagnetic calorimeter (ECAL), and a brass and scintillator hadron calorimeter (HCAL), each composed of a barrel and two endcap sections. Forward calorimeters extend the pseudorapidity coverage provided by the barrel and endcap detectors. Muons are detected in gas-ionization chambers embedded in the steel flux-return yoke outside the solenoid.

In the barrel section of the ECAL, an energy resolution of about 1% is achieved for unconverted or late-converting photons in the tens of GeV energy range. The remaining barrel photons have a resolution of about 1.3% up to $|\eta| = 1$, rising to about 2.5% at $|\eta| = 1.4$. In the endcaps, the resolution of unconverted or late-converting photons is about 2.5%, while the remaining endcap photons have a resolution of 3–4% [21].

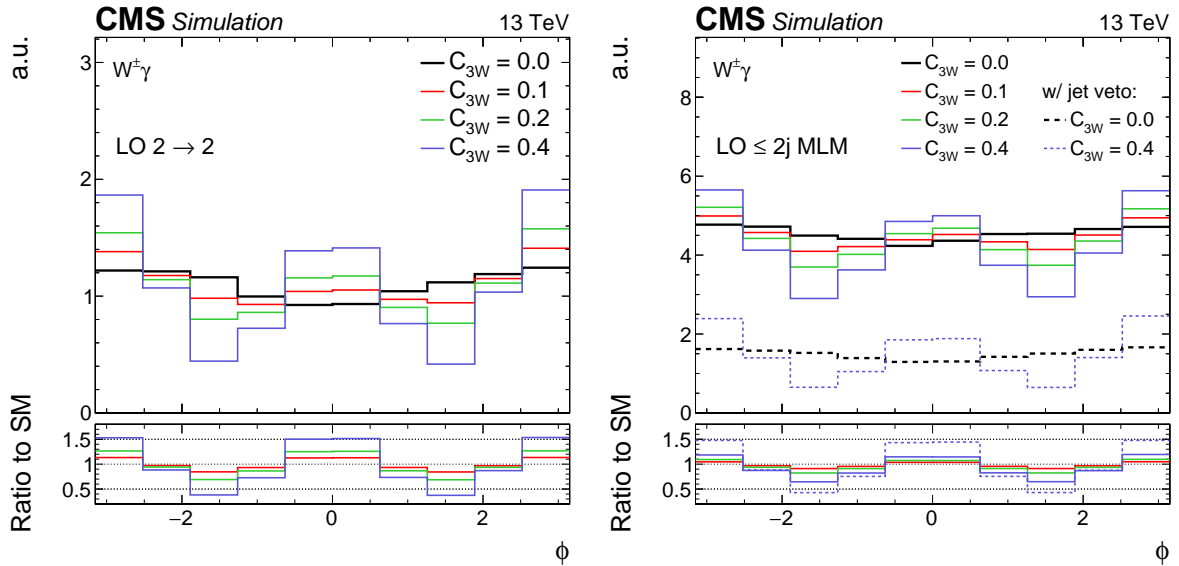


Figure 3: Particle-level distributions (in arbitrary units) of the decay angle ϕ , comparing the LO $2 \rightarrow 2$ process (left) to the LO MLM-merged prediction with up to two additional jets in the matrix element calculations (right). The black line gives the SM prediction ($C_{3W} = 0$) and the red, green, and blue lines correspond to different nonzero values of C_{3W} , for which only the interference contribution is shown. The black and blue dashed lines in the right figure give the distributions in the presence of a jet veto, as described in the text.

The electron momentum is estimated by combining the energy measurement in the ECAL with the momentum measurement in the tracker. The momentum resolution for electrons with $p_T \approx 45$ GeV from $Z \rightarrow ee$ decays ranges from 1.7 to 4.5%. It is generally better in the barrel region than in the endcaps, and also depends on the bremsstrahlung energy emitted by the electron as it traverses the material in front of the ECAL [22].

Muons are measured in the range $|\eta| < 2.4$, with detection planes made using three technologies: drift tubes, cathode strip chambers, and resistive plate chambers. Matching muons to tracks measured in the silicon tracker results in a relative p_T resolution of 1% in the barrel and 3% in the endcaps for muons with p_T up to 100 GeV. The p_T resolution in the barrel is better than 7% for muons with p_T up to 1 TeV [23].

Events of interest are selected using a two-tiered trigger system. The first level (L1), composed of custom hardware processors, uses information from the calorimeters and muon detectors to select events at a rate of around 100 kHz within a fixed latency of about 4 μ s [24]. The second level, known as the high-level trigger, consists of a farm of processors running a version of the full event reconstruction software optimized for fast processing, and reduces the event rate to around 1 kHz before data storage [25].

A more detailed description of the CMS detector, together with a definition of the coordinate system used and the relevant kinematical variables, can be found in Ref. [26].

4 Data samples and event simulation

This analysis uses pp collision data collected by the CMS experiment between 2016 and 2018 at $\sqrt{s} = 13$ TeV with an integrated luminosity of 138 fb^{-1} . Simulated event samples are used to model both the $W^\pm\gamma$ signal and several backgrounds. The $W^\pm\gamma$ signal, with up to one

additional jet, and the Z+jets, $Z\gamma$, $\gamma\gamma$, single-t+ γ , WW, WZ, and ZZ background samples are generated with MADGRAPH5_aMC@NLO [27] v2.3.3–2.6.5 at NLO in QCD. Backgrounds from $t\bar{t}$ +jets and single-t production are simulated with POWHEG v2.0 [28–33]. The $t\bar{t}\gamma$ background is simulated with MADGRAPH5_aMC@NLO v2.6.0 at LO in QCD. The effect of EFT operators on $W^\pm\gamma$ distributions is modeled using a dedicated sample generated with MADGRAPH5_aMC@NLO v2.6.7 at LO with up to two additional jets. Event weights for varying values of C_{3W} are embedded, utilizing LO matrix element reweighting [34] and the SMEFTSIM UFO model [35, 36].

The NNPDF3.1 [37] NNLO parton distribution functions (PDFs) are used in the $W^\pm\gamma$ signal simulation. The background samples use either the NNPDF3.0 [38] NLO or NNPDF3.1 NNLO PDFs. All samples are interfaced with PYTHIA v8.230 [39] for parton showering and underlying event simulation. Samples produced for the 2016 analysis use the CUETP8M1 [40] underlying event tune, with the exception of the $t\bar{t}$ samples, which use CUETP8M2T4 [41]. The 2017 and 2018 samples use the CP5 [42] tune. The CMS detector response is simulated with the GEANT4 package [43]. Additional pp interactions occurring in both the same and adjacent bunch crossings (pileup) are simulated as a set of minimum bias interactions that are mixed with the hard scattering event. In the analysis of each data-taking year the simulated events are weighted based on the number of pileup events to match the distribution measured in data.

5 Event and object reconstruction

The pp collision vertices in an event are reconstructed by grouping tracks consistent with originating at a common point in the luminous region. The candidate vertex with the largest value of summed physics-object p_T^2 is taken to be the primary pp interaction vertex. The physics objects are the jets, clustered using the anti- k_T jet finding algorithm [44, 45] with all the tracks assigned to candidate vertices as inputs, and the associated missing transverse momentum, taken as the negative vector p_T sum of those jets.

The full event reconstruction uses the particle-flow (PF) algorithm [46], which aims to reconstruct and identify each individual particle in an event, with an optimized combination of information from the various elements of the CMS detector. The energy of photons is obtained from the ECAL measurement. The energy of electrons is determined from a combination of the electron momentum at the primary interaction vertex as determined by the tracker, the energy of the corresponding ECAL cluster, and the energy sum of all bremsstrahlung photons spatially compatible with originating from the electron track. The energy of muons is obtained from the curvature of the corresponding track. The energy of charged hadrons is determined from a combination of their momentum measured in the tracker and the matching ECAL and HCAL energy deposits, corrected for the response function of the calorimeters to hadronic showers. Finally, the energy of neutral hadrons is obtained from the corresponding corrected ECAL and HCAL energies.

For each event, hadronic jets are clustered from these reconstructed particles using the infrared- and collinear-safe anti- k_T algorithm [44, 45] with a distance parameter of 0.4. The jet momentum is determined as the vector sum of all particle momenta in the jet, and is found from simulation to be, on average, within 5–10% of the true momentum over the entire p_T spectrum and detector acceptance. Pileup interactions can contribute additional tracks and calorimetric energy depositions to the jet momentum. To mitigate this effect, charged particles identified to be originating from pileup vertices are discarded, and an offset correction is applied to subtract remaining contributions. Jet energy corrections are derived from simulation to bring the measured response of jets to that of particle level jets on average. In situ measurements of

the momentum balance in dijet, photon+jet, Z+jet, and multijet events are used to correct any residual differences in the jet energy scale between data and simulation [47].

Events of interest in this analysis are characterized by the presence of a single isolated charged lepton, either an electron or a muon; an isolated photon; and missing transverse momentum. Identification and isolation criteria are used to improve the purity of events containing prompt leptons or photons, while rejecting candidates that originate from jets, pileup interactions, or misreconstruction.

The identification criteria for photons [48] include selections on the ratio of hadronic to electromagnetic energy deposited in calorimeters (H/E), a variable quantifying the lateral extension of the shower ($\sigma_{\eta\eta}$), and a requirement that the photon ECAL cluster is not matched to an electron track that has hits in the innermost tracker layers. Electron candidates are required to pass identification criteria related to the impact parameters of the track with respect to the primary vertex, the matching between the track and ECAL cluster, the shower shape in the ECAL, and the same H/E variable as for photons. A veto on electrons originating from photon conversions is applied [21]. Muon candidates are reconstructed by a simultaneous track fit to hits in the tracker and in the muon chambers. Identification criteria are applied to the impact parameters with respect to the primary vertex, to the number of spatial measurements in the silicon tracker and the muon system, and to the fit quality of the combined muon track.

Both lepton and photon candidates are required to be isolated from any other activity in the event. For electrons and muons, a relative isolation variable is defined as

$$I_{\text{rel}}^{\ell} = \frac{1}{p_T^{\ell}} \left[\sum_{\text{charged}} p_T + \max \left(0, \sum_{\text{neutral}} p_T + \sum_{\text{photons}} p_T - p_T^{\text{pileup}} \right) \right], \quad (4)$$

where the sums are over the PF candidates of the indicated type that are within $\Delta R < 0.4$ of the lepton, with $\Delta R = \sqrt{(\Delta\eta)^2 + (\Delta\phi)^2}$. To suppress the effect of pileup, only charged hadrons compatible with originating at the primary vertex are included. For the neutral hadron and photon sums, an estimate of the expected pileup contribution is subtracted [23, 48]. Requirements of $I_{\text{rel}}^{\mu} < 0.15$ and $I_{\text{rel}}^e < 0.05\text{--}0.09$ are applied, where the latter selection varies with p_T^e and $|\eta^e|$. For photons, isolation requirements are applied separately to each of the three components in Eq. (4). In addition, a selection is applied on the maximal charged particle isolation sum $I_{\text{ch}}^{\text{max}}$ computed with respect to any vertex. A requirement of $I_{\text{ch}}^{\text{max}} < \min(0.05p_T^{\gamma}, 6\text{ GeV})$ is applied. This more than halves the rate of photons from pileup jets, which constitute around 60% of misidentified photons at low p_T^{γ} .

For leptons and photons, several corrections are applied to the simulation to improve the modeling of the data. Correction factors are applied as event weights for the efficiencies of electrons and muons to be reconstructed, pass their respective identification and isolation criteria, and pass the single-lepton trigger requirements. These are determined using the “tag-and-probe” (T&P) technique [49] with $Z \rightarrow \ell\ell$ data. Similarly, scale factors for the efficiencies of photons to pass identification and isolation criteria are applied. These are measured with the T&P technique in $Z \rightarrow ee$ events, where the probe electron is reconstructed as a photon. The muon momentum scale in data and simulation is corrected using a calibration derived in $Z \rightarrow \mu\mu$ events [23, 50]. In simulation this includes an additional resolution smearing to match the performance in data. Similarly, scale and resolution corrections are applied to simulated electrons and photons to better match the data resolution.

The missing transverse momentum vector \vec{p}_T^{miss} is computed as the negative vector p_T sum of all the PF candidates in an event, and its magnitude is denoted as p_T^{miss} [51]. The \vec{p}_T^{miss}

vector is modified to account for corrections to the energy scale of the reconstructed jets. The pileup-per-particle identification algorithm [52] is applied to reduce the pileup dependence of the \vec{p}_T^{miss} observable. In the sum over PF candidates, each p_T is weighted by the probability for that particle to originate from the primary interaction vertex.

Anomalous high- p_T^{miss} events can be due to a variety of reconstruction failures, detector malfunctions, or noncollision backgrounds. Such events are rejected by event filters that are designed to identify more than 85% of the spurious high- p_T^{miss} events with a mistagging rate of less than 0.1% [51].

6 Event selection

Single-lepton triggers are used to select data events. These require that candidates pass loose identification and isolation criteria and have a p_T above thresholds of 27–32 GeV for electrons and 24–27 GeV for muons, with the exact values depending on the data-taking year.

The offline event selection requires the presence either of an electron with $p_T > 35$ GeV and $|\eta| < 2.5$ (electron channel) or a muon with $p_T > 30$ GeV and $|\eta| < 2.4$ (muon channel). The lepton must pass the identification criteria outlined in Section 5 and be spatially matched to the object that fired the trigger. Electron candidates falling in the transition region between the ECAL barrel and endcap calorimeters, $1.44 < |\eta| < 1.57$, are rejected. Events are vetoed if they contain additional leptons with $p_T > 10$ GeV that pass looser versions of the identification criteria. The same photon selection is used for both channels. The photon is required to have $p_T > 30$ GeV and $|\eta| < 2.5$, not fall in the ECAL transition region, pass the identification and isolation requirements and be separated from the selected lepton by $\Delta R > 0.7$. Events with more than one photon passing these requirements are rejected. Hadronic jets in the event are counted if having $p_T > 30$ GeV, $|\eta| < 2.5$, and a separation from both the lepton and photon of $\Delta R > 0.4$.

In both channels, events are required to have $p_T^{\text{miss}} > 40$ GeV. This reduces a large source of background from processes that do not contain any intrinsic p_T^{miss} , for example $Z \rightarrow \ell\ell$. Events with $m_{\ell\gamma}$, the invariant mass of the lepton-photon pair, close to m_Z are rejected. In the electron channel this veto is on events with $70 < m_{e\gamma} < 110$ GeV, which reduces the remaining $Z \rightarrow ee$ contribution. In the muon channel the range is $70 < m_{\mu\gamma} < 100$ GeV, which rejects events where the photon originates as final-state radiation, $Z \rightarrow \mu\mu \rightarrow \mu\mu\gamma$, and takes a large fraction of the original muon momentum.

This baseline event selection results in the selection of 72 798 electron channel and 109 669 muon channel events, of which $W^\pm\gamma$ production is expected to account for 53 and 58%, respectively. Figure 4 shows the p_T^ℓ , p_T^γ , $m_T(\ell, p_T^{\text{miss}})$, and m_T^{cluster} distributions in data and simulation, summed over the electron and muon channels. The m_T^{cluster} observable is the transverse mass of the $\ell\nu\gamma$ system, defined as

$$m_T^{\text{cluster}} = \sqrt{\left[\sqrt{m_{\ell\gamma}^2 + p_{T,\ell\gamma}^2} + p_T^{\text{miss}} \right]^2 - p_{T,\ell\gamma\text{miss}}^2}, \quad (5)$$

where $p_{T,\ell\gamma}$ is the transverse momentum of the lepton and photon system, and $p_{T,\ell\gamma\text{miss}}$ is the transverse momentum of the lepton, photon, and p_T^{miss} system. The baseline selection is used for the majority of the differential cross section measurements reported in Section 9. For the EFT analysis a tighter selection, the EFT selection, with $p_T^\ell > 80$ GeV and $p_T^\gamma > 150$ GeV is applied, and events containing hadronic jets, as defined above, are vetoed.

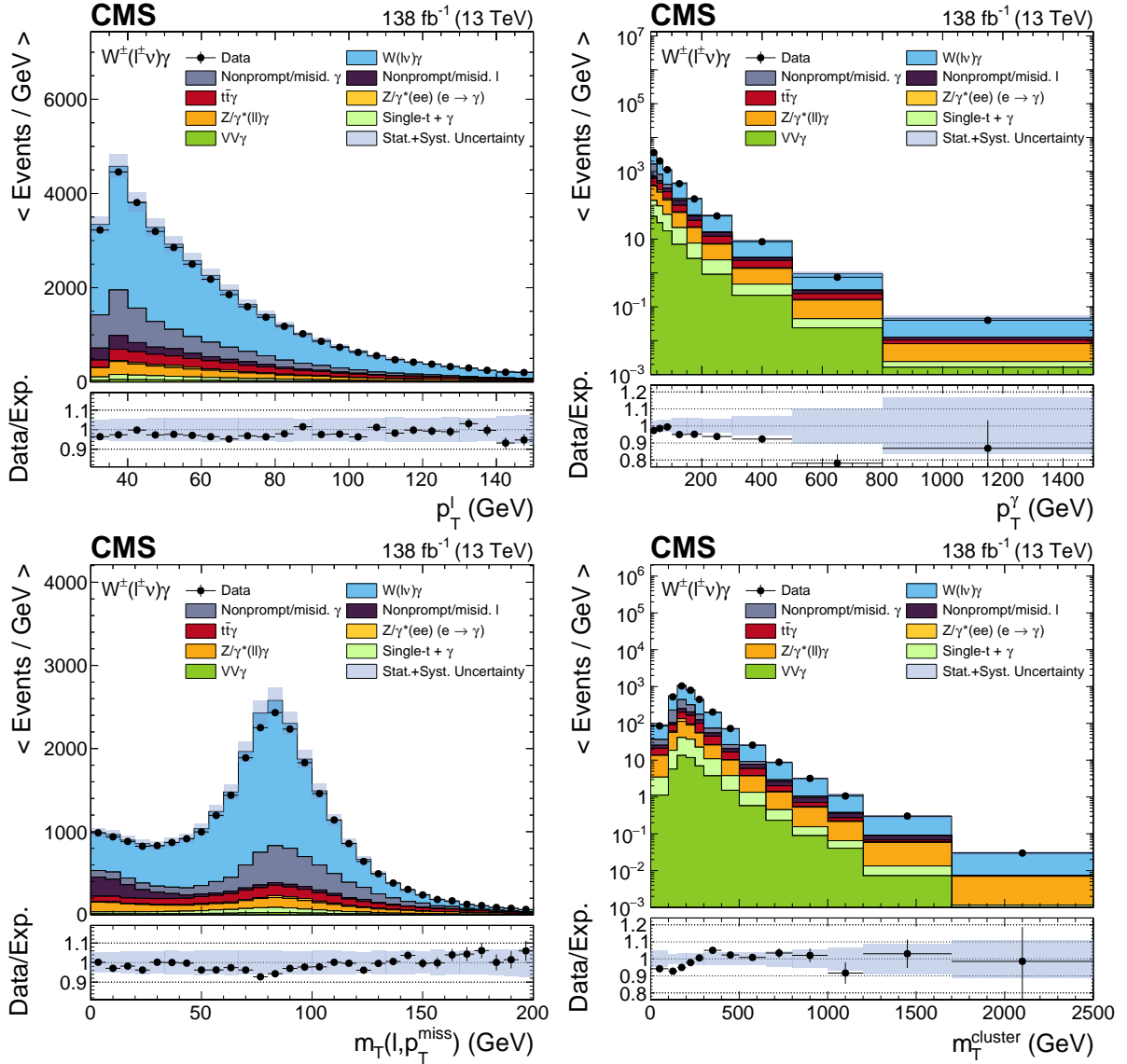


Figure 4: Distributions of the lepton p_T (upper left), the photon p_T (upper right), $m_T(\ell, p_T^{\text{miss}})$ (lower left), and m_T^{cluster} (lower right), combining the electron and muon channels. The horizontal and vertical bars associated to the data points correspond to the bin widths and statistical uncertainties, respectively. The shaded band represents the total statistical and systematic uncertainty in the signal plus background expectation.

6.1 Reconstruction of ϕ

In the EFT analysis the neutrino four-momentum is required to construct the $W^\pm\gamma$ center-of-mass frame and determine the azimuthal angle ϕ . The reconstruction procedure described in Ref. [12] is followed. The \vec{p}_T^{miss} vector in the event is assumed to be the transverse momentum of the neutrino, \vec{p}_T^ν . Then by requiring that the invariant mass of the charged lepton and neutrino system equals the W^\pm boson pole mass m_W , it is possible to form an equation for η^ν ,

$$\eta^\nu = \eta^\ell \pm \ln \left[1 + \Delta \sqrt{2 + \Delta^2 + \Delta^2} \right], \quad (6)$$

where:

$$\Delta = \sqrt{\frac{m_W^2 - m_T^2}{2 p_T^\ell p_T^\nu}}, \quad (7)$$

η^ℓ is the pseudorapidity of the lepton, and m_T is the transverse mass of the $\ell\nu$ system. Of the two possible solutions for η^ν , only one will correspond to the unknown true value. One of the two solutions is picked at random event-by-event. In the limit of high W^\pm boson momentum, it can be demonstrated that the two solutions for ϕ , ϕ^+ and ϕ^- , are related by $\phi^+ = \pi - \phi^-$, modulo 2π . This intrinsic ambiguity does not, however, prevent the observation of the interference effect. This is illustrated in Fig. 3, where the deviation in the ϕ distribution is unaffected by a transformation $\phi \rightarrow \pi - \phi$.

One additional complication to this reconstruction is in cases where $m_T > m_W$, either because the W^\pm boson was produced off shell, or because of mismeasured \vec{p}_T^{miss} in the reconstruction. In this case Eq. (6) has no real solutions and instead η^ν is assumed to equal η^ℓ , which gives a lepton-neutrino mass as close as possible to m_W . In these events ϕ is biased towards $\pm\pi/2$. Figure 5 shows the two-dimensional (2D) distribution of ϕ^{gen} versus ϕ^{true} , where ϕ^{gen} is the reconstructed ϕ angle using particle-level quantities.

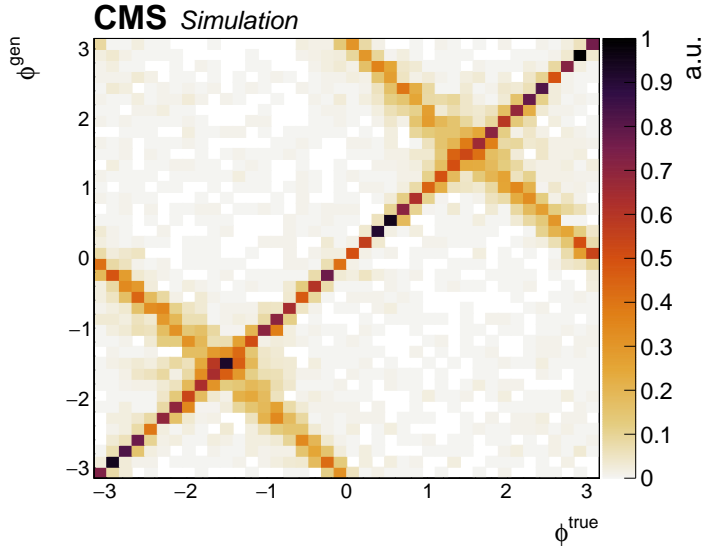


Figure 5: The two-dimensional distribution of ϕ^{gen} versus ϕ^{true} , where the former is reconstructed using the particle-level lepton and photon momenta and \vec{p}_T^{miss} . The off-diagonal components correspond to events where the incorrect solution for η^ν is chosen, as described in the text.

Given this ambiguity in ϕ , the variable ϕ_f is used in the subsequent analysis, where

$$\phi_f = \begin{cases} -(\pi + \phi), & \text{for } \phi < -\frac{\pi}{2}; \\ \phi, & \text{for } |\phi| < \frac{\pi}{2}; \\ \pi - \phi, & \text{for } \phi > \frac{\pi}{2}. \end{cases} \quad (8)$$

Furthermore, since the distributions of ϕ_f shown in Fig. 3 are symmetric about zero, the magnitude $|\phi_f|$ will be used.

7 Background estimation

The background from processes containing prompt leptons and photons is estimated from simulation. This includes $Z/\gamma^*(\ell\ell)\gamma$, $t\bar{t}\gamma$, $WV\gamma$, and single- $t+\gamma$ production, where $V = W, Z$.

An important background in the electron channel is from events with two prompt electrons, predominantly $Z \rightarrow ee$, in which one is misidentified as the photon candidate. The rate at which electrons, having passed the photon identification criteria described in Section 5, are subsequently not rejected by the specific electron veto is measured in both data and simulation using the T&P method. The probability in data is typically 1–5%, depending on the p_T and η of the electron. The resulting correction factors are applied in all simulated events where the photon candidate is matched to a prompt electron at the generator level.

The remaining backgrounds originate from other processes where one or both of the lepton and photon are misidentified, and these are discussed in the following sections.

7.1 Jets misidentified as photons

After the baseline selection, the main background in both channels comes from $W+jets$ events in which a jet is misidentified as a photon. These jets tend to have high fractions of energy deposited in the ECAL, and may contain genuine photons, for example from $\pi^0 \rightarrow \gamma\gamma$ decays. Since the probability for jets to pass the photon identification criteria is not guaranteed to be well modeled in simulation, this background is estimated using data.

Independent control regions, with a high purity in misidentified jets, are defined by inverting some of the photon identification requirements. Two variables are used: the charged isolation sum defined in Eq. (4), denoted I_{ch} , and $\sigma_{\eta\eta}$. This exploits the fact that misidentified jets tend to be less well isolated and have broader showers than prompt photons. For a given selection and observable bin, the events in the inverted- $\sigma_{\eta\eta}$ region are used to predict the number of misidentified jet events in the nominal region, N_{misid} . Each inverted- $\sigma_{\eta\eta}$ event is assigned an extrapolation factor, f_γ , corresponding to the expected inverted-to-nominal ratio given the p_T and $|\eta|$ of the photon candidate. This gives

$$N_{\text{misid}} = \sum_{\text{data}} f_\gamma(p_T^\gamma, \eta^\gamma) - N_{\text{sim}}^{\text{prompt-}\gamma}, \quad (9)$$

where the sum runs over all data events in the inverted- $\sigma_{\eta\eta}$ region, and $N_{\text{sim}}^{\text{prompt-}\gamma}$ is the estimated prompt photon contamination, determined by applying the same extrapolation factors to simulated events in this region. The f_γ value for each p_T and $|\eta|$ bin is determined from a region where I_{ch} is inverted. The $\sigma_{\eta\eta}$ extrapolation factor, calculated after the subtraction of the expected prompt photon contribution, varies linearly with I_{ch} . Therefore, a linear fit to the ratio is performed, with the result extrapolated to the nominal I_{ch} region to give f_γ .

The statistical uncertainty in f_γ is 2–35%, depending on the p_T and $|\eta|$ bin. Systematic uncertainties come from the normalization of the prompt photon contribution that is subtracted, and the bias in the extrapolated value of f_γ , compared with the true value, when the method is validated in simulation. The former is typically 10%, and the latter is up to 15% in a given bin. The total statistical and systematic uncertainty, which ranges from 10 to 45%, is propagated through all subsequent results.

In the EFT selection, because of the limited number of control region events for $p_T^\gamma > 150 \text{ GeV}$, this method is modified. In the inverted- $\sigma_{\eta\eta}$ region, the nominal requirement on I_{ch} is retained, whereas all other photon identification criteria are removed and replaced with only a loose requirement of $H/E < 0.15$. The total uncertainty in f_γ is 20–60% under this selection, and the statistical component is typically dominant.

7.2 Misidentified leptons

Another contribution comes from events with a prompt photon but a nonprompt or misidentified lepton, e.g., within a jet containing a semileptonic meson decay. The main identifying feature of such events is that the leptons will generally be less well isolated. The contribution is estimated by applying an inverted lepton isolation requirement, and applying a per-event extrapolation factor f_ℓ , binned in p_T and $|\eta|$, to predict the number of events in the nominal isolated selection.

The f_ℓ factors are measured in a control region in data designed to increase the purity of events with misidentified leptons. This control region is obtained by applying the baseline selection in both channels, but vetoing the presence of an identified photon and instead requiring the presence of a jet with $p_T > 30 \text{ GeV}$ and $|\eta| < 2.5$. A requirement of $m_T(\ell, p_T^{\text{miss}}) < 30 \text{ GeV}$ is applied to reject the background from W+jets events. The remaining contamination from W+jets and other prompt-lepton sources is estimated using simulation and subtracted. The normalization uncertainty in this prompt subtraction dominates the uncertainties in the f_ℓ factors, which are typically 10–40%.

Both the misidentified lepton and misidentified photon background estimates predict the contribution from events where both objects are misidentified. To avoid double-counting these events, their expected contribution is subtracted from the misidentified lepton background estimate. This is estimated using events in a region where both the lepton isolation and photon $\sigma_{\eta\eta}$ requirements are inverted, where the extrapolation factors for both methods are applied.

8 Systematic uncertainties

The effects of systematic uncertainties in the signal and background expectations are incorporated for all measurements in this analysis. The majority of the uncertainties affect both the shape and normalization of the predictions, whereas several affect only the normalization. The shape variations are modeled by a smooth interpolation between the nominal and ± 1 standard deviation predictions in each bin and a linear extrapolation beyond this. The systematic uncertainties and their typical effect on the expected yields are summarized in Table 1. The experimental sources are as follows:

- *Integrated luminosity:* The 2016, 2017, and 2018 data set uncertainties are 1.2%, 2.3%, and 2.5% [53–55], respectively, applied to all processes estimated purely with simulation. The total integrated luminosity has an uncertainty of 1.6%, the improvement in precision reflecting the (uncorrelated) time evolution of some systematic effects.

Table 1: Summary of the systematic uncertainties affecting the signal and background predictions. The table notes whether each uncertainty affects the shape of the measured observable or just the normalization (Affects shape), and whether the effect is correlated between the data-taking years (Corr. years). The normalization effect on the expected yield of the applicable processes is also given. For some shape uncertainties the values vary significantly across the observable distribution. In these cases the typical range and maximum values are given, where the former is the central 68% interval considering all bins.

Uncertainty	Affects shape	Corr. years	Relative effect on expected yield
<i>Experimental</i>			
Integrated luminosity	—	Partial	1.6%
Pileup modeling	✓	✓	0.2–3.1%
L1 trigger	✓	✓	0.3–1.1%
Electron ID	✓	✓	0.7–2.8%
Electron ID ($p_T^e > 200 \text{ GeV}$)	✓	—	0.1–1.2%
Electron trigger	—	—	0.5%
Muon ID (stat)	✓	—	0.1–0.6%
Muon ID (syst)	✓	✓	0.2–0.7%
Muon trigger	✓	—	0.1–0.7%
Photon ID	✓	✓	0.6–6.0%
Photon ID ($p_T^\gamma > 200 \text{ GeV}$)	✓	—	2.1–4.7%
Photon ID (high p_T extrapolation)	✓	—	Typically 3.0–9.0%, max. 14%
Photon (e veto)	—	—	1%
Photon energy scale	✓	✓	Typically 0.1–4.8%, max. 13%
Jet energy scale	✓	—	1–4%
p_T^{miss} scale	✓	Partial	0.1–10.1%
$e \rightarrow \gamma$ misidentification	✓	—	Typically 6.7–18%, max. 25%
Jet $\rightarrow \gamma$ misidentification	✓	—	10–45%
Misidentified e	✓	—	Typically 13–36%, max. 75%
Misidentified μ	✓	—	Typically 16–42%, max. 70%
<i>Theoretical</i>			
$W^\pm \gamma$ acceptance (scale)	✓	✓	0.3–1.7%
$W^\pm \gamma$ acceptance (PDF)	✓	✓	Typically 0.5–2.2%, max. 7.6%
$W^\pm \gamma$ out-of-acceptance (scale)	✓	✓	5.2–12%
$W^\pm \gamma$ parton shower modeling	✓	✓	0.2–1.3%
Background normalization (scale)	—	✓	2.0–16%
Background normalization (PDF)	—	✓	4.2–4.8%

- *Pileup modeling:* The uncertainty in the weighting of the pileup distribution in simulation is derived by varying the total inelastic cross section by $\pm 5\%$ in the estimate of the distribution in data [56].
- *L1 trigger:* During the 2016 and 2017 data-taking periods, a gradual shift in the timing of the inputs of the ECAL L1 trigger in the $|\eta| > 2.4$ region led to a specific inefficiency. A correction amounting to 2–3% is applied to the simulation along with the corresponding uncertainty in the inefficiency measurement.
- *Lepton ID and trigger efficiencies:* The uncertainties in the measured correction factors are applied to the simulation, which include both statistical and systematic sources. The latter dominate at low p_T and the former in the higher p_T range probed in this analysis.
- *Photon ID efficiency:* The uncertainties in the identification correction factors, derived in $Z \rightarrow ee$ events, are applied to the simulation. The highest p_T measurement bin ($p_T^\gamma > 200 \text{ GeV}$) is dominated by the statistical uncertainty and so is uncorrelated from the uncertainty at lower p_T . An uncertainty in the extrapolation of the efficiencies to the maximum p_T^γ considered, 1.5 TeV, is also included.
- *Photon energy scale:* The uncertainty from the calibration of the scale in data is determined using $Z \rightarrow ee$ events. Typical values are 0.1–3% of the photon energy depending on p_T .
- *Jet energy scale corrections:* The energies of jets in simulation are varied within the uncertainties of the scale correction measurements and propagated to all relevant observables. The magnitude varies with p_T and η , and is typically a few percent.
- *p_T^{miss} scale:* The uncertainty in the jet energy scale also has a correlated effect on the p_T^{miss} calculation. An additional uncertainty is included for the energy scale of PF candidates not clustered in jets.
- *Electrons misidentified as photons:* An uncertainty in the correction of the electron to photon misidentification rate, due to the subtraction of genuine photon events in the T&P measurement, is derived.
- *Jets misidentified as photons:* For jets misidentified as photons, the uncertainties from the method based on control samples in data described in Section 7.1 are applied, independently for each p_T^γ and $|\eta^\gamma|$ bin that f_γ is measured in. These uncertainties are correlated between the electron and muon channels.
- *Misidentified leptons:* The dominant source of uncertainty in the f_ℓ measurement, described in Section 7.2, comes primarily from the normalization of the subtracted prompt lepton contamination in the measurement region.
- *Simulated sample size:* The statistical uncertainty due to the finite number of simulated events per bin is applied following the Barlow–Beeston method [57].

Theoretical uncertainties in the $W^\pm\gamma$ signal prediction because of missing higher orders in the perturbative cross section calculation are evaluated by varying the renormalization and factorization scales, denoted μ_R and μ_F , respectively, in simulated events by factors of 0.5 and 2. The maximum variation among all possible pairings of μ_R and μ_F is considered, with the exception of the (0.5, 2) and (2, 0.5) combinations. For constraints on C_{3W} , the full uncertainty from this procedure is applied, which amounts to an 8–11% normalization effect depending on the bin. For the cross section measurements, the effect on the predicted cross sections is neglected, whereas the effect on the reconstruction-level acceptance is retained. These values typically vary from 0.5 to 2% and are treated as independent for each measured cross section

bin. Conversely, for the contamination of signal events from outside the fiducial region, the effect on both cross section and acceptance is included. Uncertainties from the NNPDF3.1 PDF set eigenvectors are also evaluated following the PDF4LHC prescription [58], and affect the acceptance by up to 2%. For measurements that include a jet veto, an additional migration uncertainty between the 0-jet and ≥ 1 -jet regions is applied, following the procedure described in Ref. [59]. This results in an 8.6% uncertainty in the 0-jet cross section.

Normalization uncertainties are assigned for each background process estimated with simulation to account for missing higher-order corrections and the PDF choice. These are treated as uncorrelated between different processes, and are calculated following the same procedures as for the signal. The missing higher-order correction uncertainties typically range from 2 to 3.5%, and the PDF uncertainties are up to 4.8%, depending on process.

9 Results

The results described in this section are obtained using statistical procedures developed by the ATLAS and CMS Collaborations, detailed in Refs. [60, 61] and implemented in the ROOFIT [62] and ROOSTATS [63] frameworks.

The parameters of interest $\vec{\alpha}$ for a particular result are estimated with their corresponding confidence intervals using a profile likelihood ratio test statistic $q(\vec{\alpha})$ [64], in which experimental and theoretical uncertainties are incorporated via nuisance parameters (NPs) $\vec{\theta}$:

$$q(\vec{\alpha}) = -2 \ln \left(\frac{\mathcal{L}(\vec{\alpha}, \hat{\vec{\theta}}_{\vec{\alpha}})}{\mathcal{L}(\hat{\vec{\alpha}}, \hat{\vec{\theta}})} \right). \quad (10)$$

The asymptotic approximation, whereby $q(\vec{\alpha})$ is assumed to follow a χ^2 distribution, is used in the determination of the confidence intervals. The likelihood functions in the numerator and denominator of Eq. (10) are constructed using products of binned signal and background probability density functions, as well as constraint terms for the NPs. The quantities $\hat{\vec{\alpha}}$ and $\hat{\vec{\theta}}$ denote the unconditional maximum likelihood estimates of the parameter values, while $\hat{\vec{\theta}}_{\vec{\alpha}}$ denotes the conditional maximum likelihood estimate for fixed values of the parameters of interest $\vec{\alpha}$. The binned likelihood function is expressed as

$$\mathcal{L}(\text{data} | \vec{\alpha}, \vec{\theta}) = \prod_i \text{Poisson}(n_i | s_i(\vec{\alpha}, \vec{\theta}) + b_i(\vec{\theta})) p(\tilde{\vec{\theta}} | \vec{\theta}), \quad (11)$$

where n_i is the number of observed events in each bin, s and b are the expected numbers of signal and background events, and $\tilde{\vec{\theta}}$ represents the nominal values of the NPs, determined by external measurements.

For the measurement of a set of fiducial cross sections, $\vec{\alpha} \equiv \sigma_j$, the signal expectation s is constructed as

$$s_i = \sum_j \sigma_j R_{ij}(\vec{\theta}) L + \sum_k \sigma_k^{\text{OOA}} R_{ik}(\vec{\theta}) L, \quad (12)$$

where j runs over the set of $W^\pm\gamma$ fiducial cross sections being measured; k runs over a set of unmeasured fiducial cross section bins, referred to as out-of-acceptance (OOA) and discussed further below; L is the integrated luminosity of a given data set; and R_{ij} is the response matrix, parameterized by $\vec{\theta}$, giving the probability for an event in fiducial bin j to be reconstructed in analysis bin i .

In this measurement a significant OOA contribution can come from events that are within the fiducial acceptance with the sole exception of the p_T^{miss} requirement, because p_T^{miss} is measured with poor resolution compared with the transverse momentum of the leptons and photons. This component is therefore split into the same set of fiducial bins j but with a modified p_T^{miss} selection. Since it is not possible to measure these OOA cross sections σ_j^{miss} simultaneously, they are related to the σ_j using the predicted ratios from the $W^\pm\gamma$ simulation: $\sigma_j^{\text{miss}} = (\sigma_j^{\text{miss,MC}} / \sigma_j^{\text{MC}}) \sigma_j$. The remaining OOA contribution σ^{OOA} is small and is fixed to the value predicted by the simulation. This includes events in which the electron or muon originates from a tau lepton decay. Equation (12) above can then be expressed as

$$s_i = \sum_j \left[\sigma_j R_{ij}(\vec{\theta}) L + \frac{\sigma_j^{\text{miss,MC}}}{\sigma_j^{\text{MC}}} \sigma_j R_{ij}^{\text{miss}}(\vec{\theta}) L \right] + \sigma^{\text{OOA}} R_i^{\text{OOA}}(\vec{\theta}) L. \quad (13)$$

In addition to measuring the absolute σ_j , it is useful to present the results as fractional cross sections, $f_j = \sigma_j / \sigma_{\text{tot}}$, where σ_{tot} is treated as a free parameter in the likelihood fit and $\sum f_j$ is constrained to unity. This facilitates comparisons between different predictions purely on the basis of observable shape, and reduces the impact of systematic uncertainties that are uniform across the distribution, for example from the integrated luminosity.

Tabulated versions of all the results in this section are provided in the HEPData record for this analysis [65].

9.1 Differential cross sections

The differential cross sections $\sigma_j(p p \rightarrow W^\pm\gamma \rightarrow \ell^\pm\nu\gamma)$, where ℓ denotes all three lepton flavors, are measured in the following fiducial region:

- $p_T^\ell > 30 \text{ GeV}$, $|\eta^\ell| < 2.5$,
- $p_T^\gamma > 30 \text{ GeV}$, $|\eta^\gamma| < 2.5$,
- $p_T^{\text{miss}} > 40 \text{ GeV}$,
- $\Delta R(\ell, \gamma) > 0.7$.

These selections are chosen to match as closely as possible with the reconstruction-level baseline described in Section 6, with two exceptions: in the electron channel $p_T^e > 35 \text{ GeV}$ is required because of the higher trigger thresholds, and in the muon channel $|\eta^\mu| < 2.4$ is applied to reflect the acceptance of the muon system.

The lepton momenta are completed by adding the four-momenta of any photons with $\Delta R(\ell, \gamma) < 0.1$ to the four-momentum of the lepton. A smooth-cone photon isolation selection is also applied. This is necessary to ensure an infrared-safe cross section calculation in perturbative QCD. It requires that for every cone in η - ϕ around the photon direction with radius $\delta < \delta_0$ the total scalar transverse energy sum E_T must be smaller than $E_T^{\max}(\delta)$ [66] where

$$E_T^{\max}(\delta) = \epsilon p_T^\gamma \left(\frac{1 - \cos \delta}{1 - \cos \delta_0} \right)^n, \quad (14)$$

and the values of the tunable parameters are set as $\delta_0 = 0.4$, $\epsilon = 1.0$, and $n = 1$.

Differential cross sections are measured for p_T^γ , η^γ , $\Delta R(\ell, \gamma)$, $\Delta\eta(\ell, \gamma)$, and m_T^{cluster} under the baseline selection. The $|\phi_f|$ observable is measured only under the higher- p_T EFT selection, given in Section 9.4, where the resolution is sufficiently improved compared to the baseline selection.

The signal model is constructed as in Eq. (13), where the OOA contributions σ_j^{miss} are defined for events with $0 < p_T^{\text{miss}} < 40 \text{ GeV}$, but otherwise within the fiducial region for j . A simultaneous fit is performed to the reconstructed distributions of the observables in each year and for each of the electron and muon channels, where lepton flavor universality in the W boson decay is assumed. These distributions use the same bin boundaries as the fiducial-level cross section bins. The measurements are compared with the predictions from the NLO MADGRAPH5_aMC@NLO+PYTHIA simulation (MG5_aMC+PY8) and NNLO predictions from the MATRIX [67, 68], MCFM [69, 70], and GENEVA [71–74] frameworks.

The MATRIX calculation implements a dedicated q_T -subtraction formalism [75, 76], where q_T is the total transverse momentum of the colorless final state particles. The framework utilizes amplitudes up to one-loop level from OPENLOOPs [77, 78], as well as dedicated two-loop calculations [79]. The MCFM prediction uses the N -jettiness slicing method, with all one- and two-loop amplitudes [79] calculated using analytic formulae. It is given with and without the inclusion of NLO electroweak corrections, which have been shown [69, 80] to modify $W^\pm\gamma$ differential distributions by $\mathcal{O}(10\%)$. The NLO electroweak correction to the $q\bar{q}$ -initiated process is applied multiplicatively to the NNLO QCD cross section, which is then summed with the contribution from the distinct photon-induced $q\gamma$ channel. The GENEVA framework combines the fixed-order NNLO result with a next-to-next-to-leading logarithmic resummed calculation, in this case using soft-collinear effective theory to resum the 0-jettiness variable. The output events are interfaced with PYTHIA8 [39] for parton showering, hadronization and underlying event simulation.

Figures 6–8 show the resulting measurements for each observable. For p_T^γ in Fig. 6, the uncertainty composition and correlation matrices are also given.

The absolute cross section, as a function of p_T^γ , is measured with a precision of 4–5% at low p_T , dominated by experimental systematic uncertainties, to 40% in the highest bin, dominated by the statistical uncertainty. The fractional cross section uncertainty falls to 2–3% at low p_T , owing to a cancellation of systematic uncertainties. Both measurements show a tendency towards the lower values of the NNLO predictions at high p_T . Although the NLO electroweak correction is predicted to reduce the cross section in this region by up to 30%, the current precision is not sufficient to distinguish this effect. The correlation matrices illustrate how large positive correlations between bins in the absolute measurement are reduced significantly when using the fractional parameterization.

The $\Delta R(\ell, \gamma)$ measurement is in agreement with all the predictions in the bulk of the distribution, but favors the higher NNLO predictions in the $\Delta R > 4.0$ region. The $\Delta\eta(\ell, \gamma)$ measurement shows significant enhancement in the highest $|\Delta\eta|$ bins compared with the MG5_aMC+PY8 prediction. The NNLO predictions feature a similar, though less pronounced effect. The m_T^{cluster} distribution is broadly in agreement with the predictions, however with a moderate disagreement in the shape of the peak in the 100–300 GeV region.

9.2 Cross section as a function of the jet multiplicity

The cross section is measured as a function of the jet multiplicity using the same fiducial region as the previous results. The fiducial selection for the jets is chosen to match the experimental selection. Jets are clustered from final state particles, excluding neutrinos, with the anti- k_T algorithm and a distance parameter of 0.4. They are required to have $p_T > 30 \text{ GeV}$, $|\eta| < 2.5$, and be separated from both the lepton and photon by $\Delta R > 0.4$. The measured cross sections and their correlation matrix are shown in Fig. 9, and the cross section values are listed in Table 2.

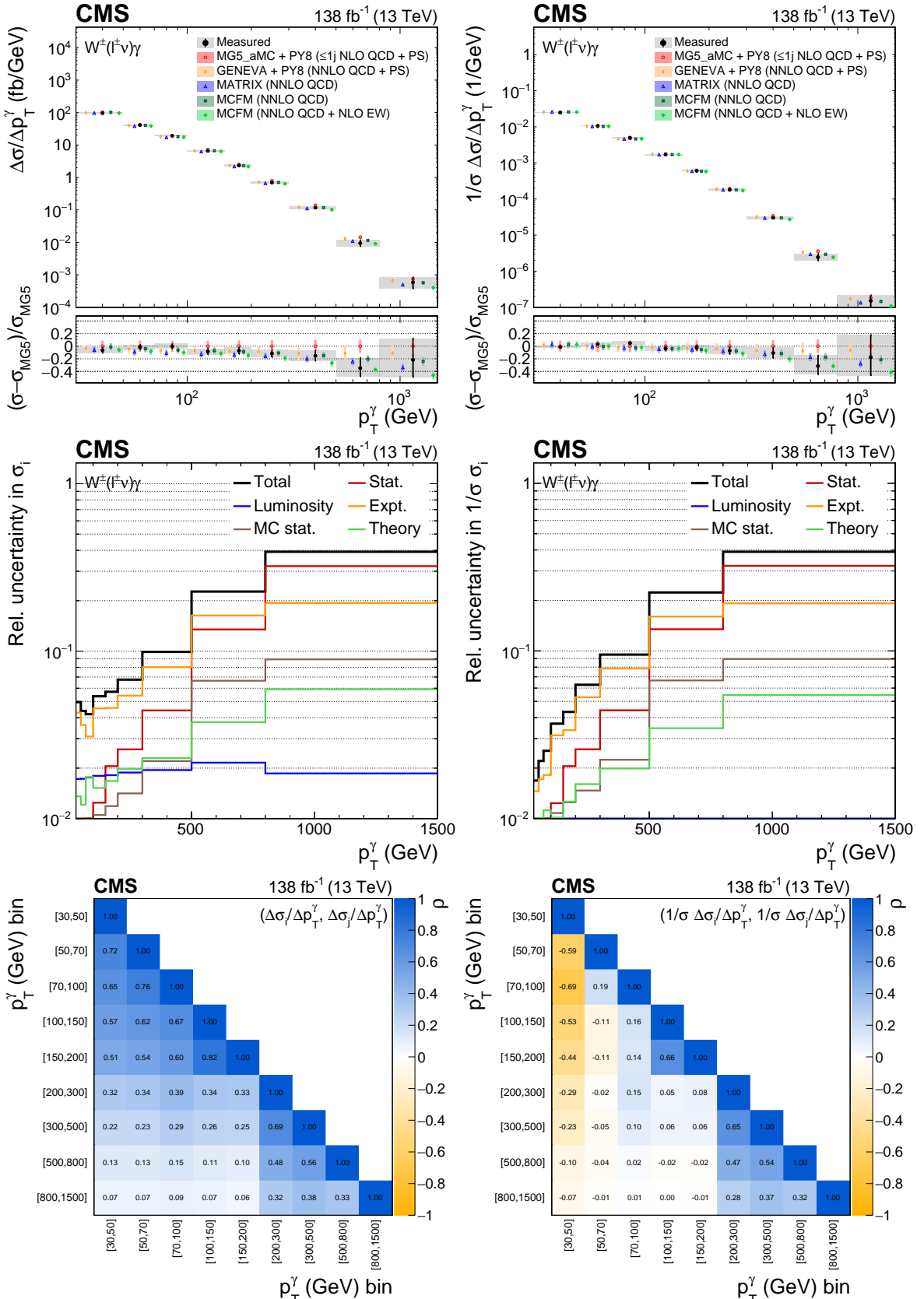


Figure 6: The measured p_T^γ absolute (left) and fractional (right) differential cross sections (upper), compared with the MG5_aMC+PY8, GENEVA, MATRIX, and MCFM predictions, and corresponding uncertainty decomposition (center) and correlation matrices (lower). In the upper figures, the black vertical bars give the total uncertainty on each measurement. The predictions are offset horizontally in each bin to improve visibility, and the corresponding vertical bars show the missing higher-order correction uncertainties.

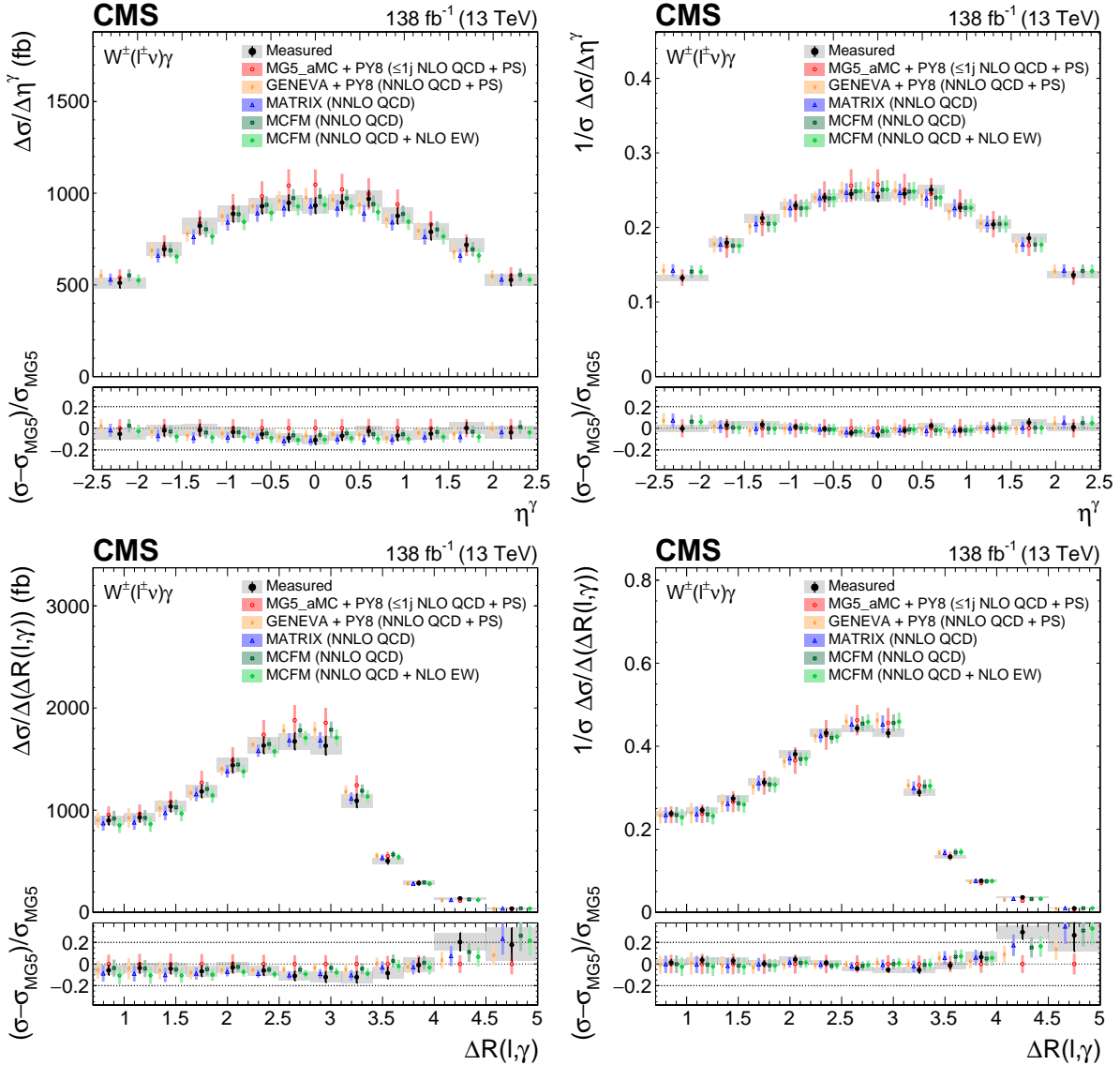


Figure 7: The measured absolute (left) and fractional (right) differential cross sections for η^γ (upper) and $\Delta R(l, \gamma)$ (lower), compared with the MG5_aMC+PY8, GENEVA, MATRIX, and MCFM predictions. The black vertical bars give the total uncertainty on each measurement. The predictions are offset horizontally in each bin to improve visibility, and the corresponding vertical bars show the missing higher-order correction uncertainties.

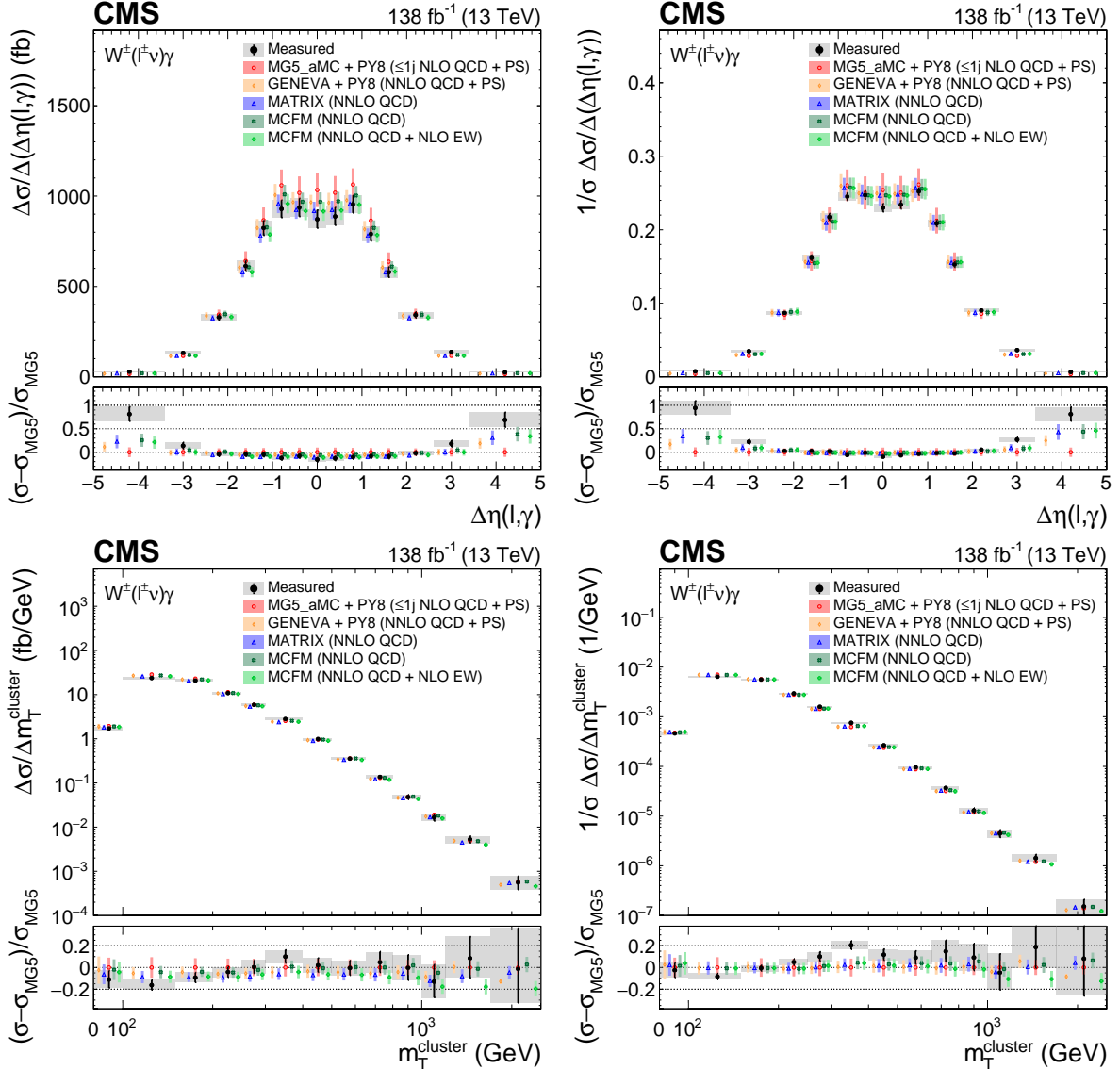


Figure 8: The measured absolute (left) and fractional (right) differential cross sections for $\Delta\eta(\ell, \gamma)$ (upper) and m_T^{cluster} (lower), compared with the MG5_aMC+PY8, GENEVA, MATRIX, and MCFM predictions. The black vertical bars give the total uncertainty on each measurement. The predictions are offset horizontally in each bin to improve visibility, and the corresponding vertical bars show the missing higher-order correction uncertainties.

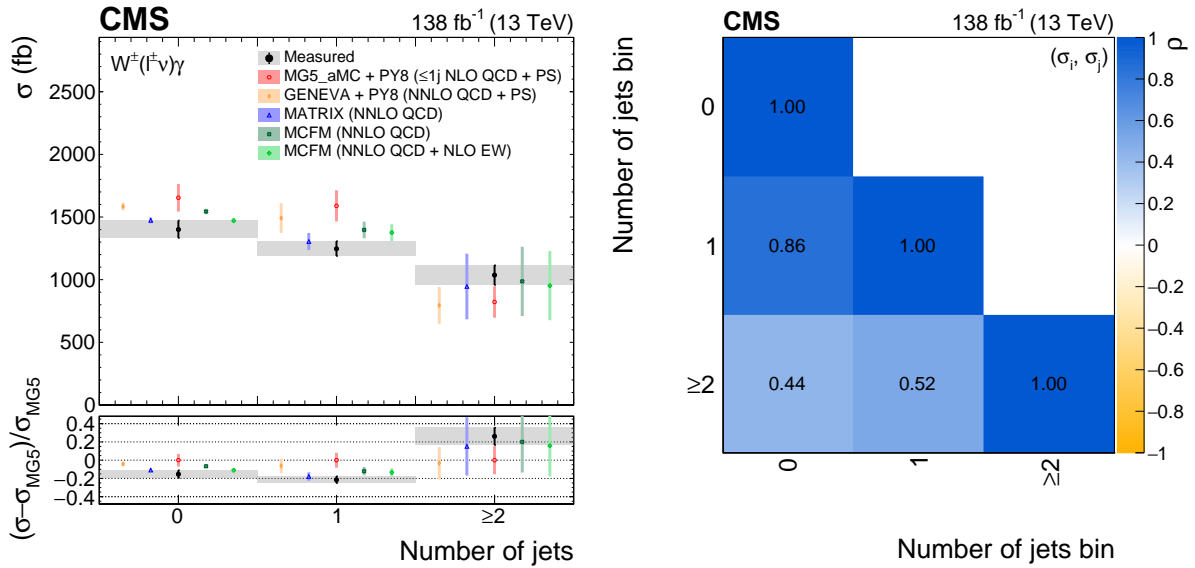


Figure 9: The measured jet multiplicity cross sections (left) and corresponding correlation matrix (right). In the left figure, the black vertical bars give the total uncertainty on each measurement. The predictions are offset horizontally in each bin to improve visibility, and the corresponding vertical bars show the missing higher-order correction uncertainties.

Table 2: Cross sections measured in bins of jet multiplicity and comparison with the MG5_aMC+PY8, GENEVA, MATRIX, and MCFM predictions. The MCFM column marked (EW) is the NNLO QCD prediction combined with NLO electroweak corrections, as described in the text.

Number of jets	$\sigma(\text{fb})$								
	Best fit	Stat	Syst	MG5_aMC+PY8	MATRIX	MCFM	MCFM (EW)	GENEVA	
= 0	1400 ⁺⁷¹ ₋₆₇	⁺¹¹ ₋₁₁	⁺⁷⁰ ₋₆₇	1650 ± 110	1473 ± 19	1544 ± 18	1471 ± 18	1584 ± 26	
= 1	1246 ⁺⁶¹ ₋₅₈	⁺¹¹ ₋₁₁	⁺⁶⁰ ₋₅₇	1590 ± 120	1304 ± 64	1397 ± 62	1376 ± 62	1490 ± 110	
≥ 2	1037 ⁺⁷⁸ ₋₇₉	⁺¹⁰ ₋₁₀	⁺⁷⁷ ₋₇₈	820 ± 120	950 ± 260	990 ± 270	950 ± 270	790 ± 140	

The measured 0-jet cross section is 5–15% smaller than the various predictions. A similar trend is observed in the 1-jet measurement, whereas the ≥ 2 -jet measurement is higher than the predictions. Each measurement is positively correlated with the other two, with the strongest correlation of +0.86 between the 0-jet and 1-jet bins.

9.3 The radiation amplitude zero effect

In pp collisions the RAZ effect is observed [4] in the rapidity difference between the charged lepton and the photon; it manifests itself as a suppression of the cross section near $\Delta\eta(\ell, \gamma) = 0$. This region is of interest because new physics effects could make the minimum in this region less pronounced. Several models with resonances that would exhibit this feature are discussed in Ref. [81]. In the EFT framework this enhancement is generated by C_{3W} , however, the $\Delta\eta(\ell, \gamma)$ observable is significantly less sensitive than the approach pursued in this paper, as described in Section 2.

To observe the RAZ effect in data it is necessary to add further requirements to the baseline selection. A veto on the presence of any jet with $p_T > 30 \text{ GeV}$ and $|\eta| < 2.5$ is applied to preferentially select events in the Born configuration, and a requirement that $m_T^{\text{cluster}} >$

150 GeV. Figure 10 shows the differential cross section measurements, where a pronounced dip at $\Delta\eta(\ell, \gamma) = 0$ is observed. The jet veto in this selection gives a similar difference in normalization between measurement and predictions as for the 0-jet cross section in the previous section. In addition, the dip at $\Delta\eta(\ell, \gamma) = 0$ is larger than the predictions, though closer to the NNLO calculations, and the enhancement in the high $|\Delta\eta(\ell, \gamma)|$ region is similar to that observed under the baseline selection in Fig. 8.

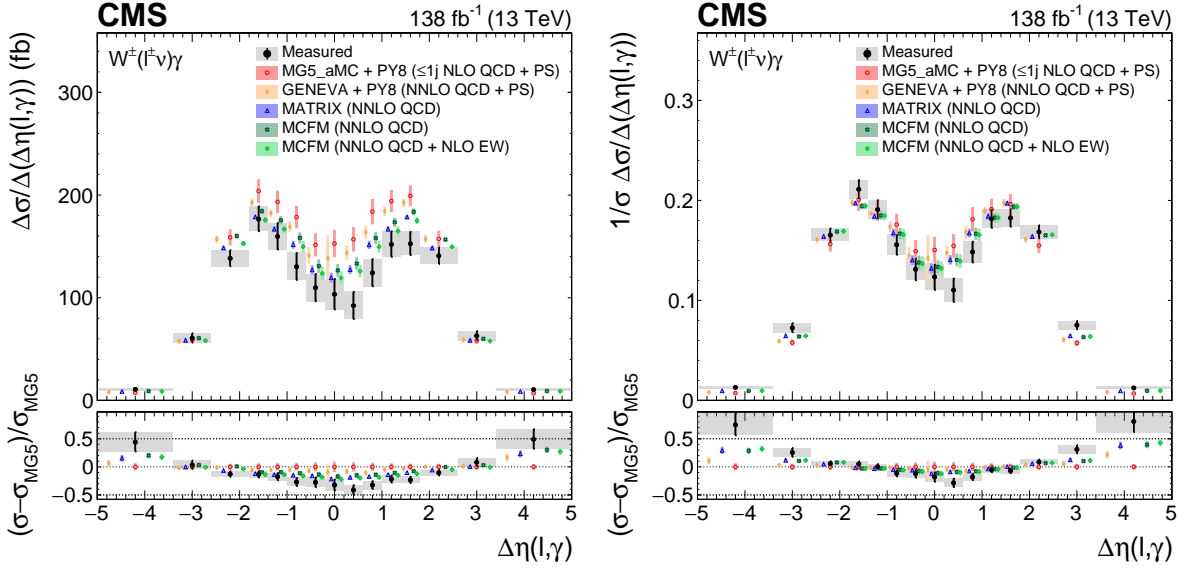


Figure 10: The measured $\Delta\eta(\ell, \gamma)$ absolute (left) and fractional (right) differential cross sections, compared with the MG5_aMC+PY8, GENEVA, MATRIX, and MCFM predictions. The black vertical bars give the total uncertainty on each measurement. The predictions are offset horizontally in each bin to improve visibility, and the corresponding vertical bars show the missing higher-order correction uncertainties.

9.4 EFT constraints

In this section, constraints on the C_{3W} coefficient are derived via a parameterization of the fiducial cross section in p_T^γ and $|\phi_f|$, under the EFT selection described in Section 6. The bin boundaries are [150, 200, 300, 500, 800, 1500] GeV and $[0, \pi/6, \pi/3, \pi/2]$, respectively. For the corresponding 2D differential cross section measurement the two highest p_T bins are merged, owing to the small number of events expected in the highest bin. As for the one-dimensional (1D) differential measurements the signal model is constructed following Eq. (13), where j runs over all p_T^γ and $|\phi_f|$ bins.

Constraints on C_{3W} are determined by parameterizing the fiducial cross section in each bin according to Eq. (3). Table 3 shows the corresponding values of the σ^{int} and σ^{BSM} terms, relative to σ^{SM} .

Figure 11 shows the expected and observed distributions, summed over the electron and muon channels, before the maximum likelihood fit is performed. The change in the expected distribution when C_{3W} is set to either -0.2 or 0.2 TeV $^{-2}$ is also shown, considering only the SM and interference terms in Eq. (3).

The 95% confidence level (CL) intervals on C_{3W} are calculated using the asymptotic properties of the profile likelihood ratio of Eq. (10). Figure 12 shows scans of this ratio as a function of C_{3W} . The intervals are $[-0.062, 0.052]$ TeV $^{-2}$ with the inclusion of the pure BSM term in Eq. (3) and $[-0.38, 0.17]$ TeV $^{-2}$ with only the SM and interference terms. The observation is therefore

Table 3: Coefficients of the fiducial cross section scaling terms in all $p_T^\gamma \times |\phi_f|$ bins. Values are given relative to the SM prediction: $\mu^{\text{int}} = \sigma^{\text{int}}/\sigma^{\text{SM}}$ and $\mu^{\text{BSM}} = \sigma^{\text{BSM}}/\sigma^{\text{SM}}$, with the total relative normalization defined as $1 + C_{3W}\mu^{\text{int}} + C_{3W}^2\mu^{\text{BSM}}$.

p_T^γ bin (GeV)	$0 \leq \phi_f < \pi/6$ μ^{int}	$0 \leq \phi_f < \pi/6$ μ^{BSM}	$\pi/6 \leq \phi_f < \pi/3$ μ^{int}	$\pi/6 \leq \phi_f < \pi/3$ μ^{BSM}	$\pi/3 \leq \phi_f < \pi/2$ μ^{int}	$\pi/3 \leq \phi_f < \pi/2$ μ^{BSM}
150–200	−0.19	0.52	0.03	0.50	0.23	0.44
200–300	−0.38	2.5	0.02	2.1	0.43	1.9
300–500	−0.95	10.7	0.06	10.3	1.0	11.0
500–800	−2.2	83.0	0.07	82.5	2.4	81.6
800–1500	−4.9	688.5	0.02	651.7	4.9	646.2

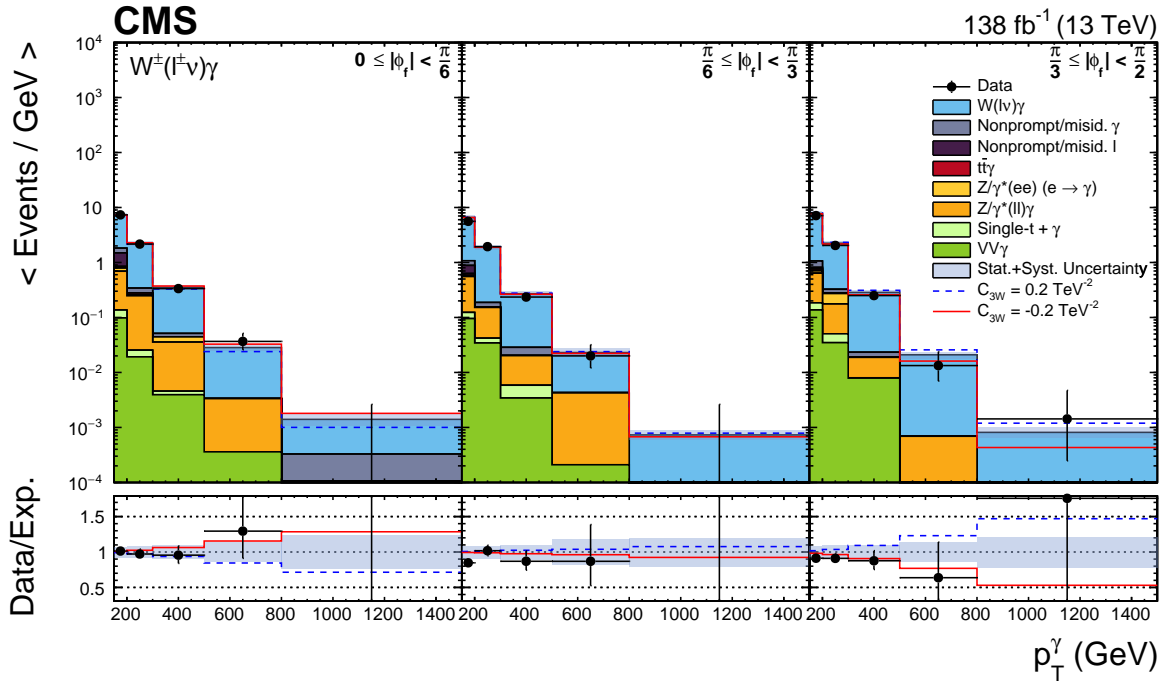


Figure 11: The expected and observed p_T^γ distribution in each $|\phi_f|$ region before the maximum likelihood fit is performed, combining the electron and muon channels. The horizontal and vertical bars associated to the data points correspond to the bin widths and statistical uncertainties, respectively. The shaded uncertainty band incorporates all statistical and systematic uncertainties. The red and blue lines show how the total expectation changes when C_{3W} is set to -0.2 and 0.2 TeV^{-2} , respectively. Only the SM and interference terms are included in this example.

compatible with the SM prediction of $C_{3W} = 0$. Constraints are also determined as a function of the maximum p_T^γ bin that is included in the fit, shown in Fig. 13 (left) and Table 4. Such a presentation is useful for interpretations where the highest bins may be beyond the validity of the EFT or specific BSM model being tested [82]. These constraints are also determined with and without the inclusion of the pure BSM term. This shows that with the current amount of data the pure BSM term dominates for all values of the cutoff. However, the sensitivity to the interference term is comparable at lower values of p_T^γ .

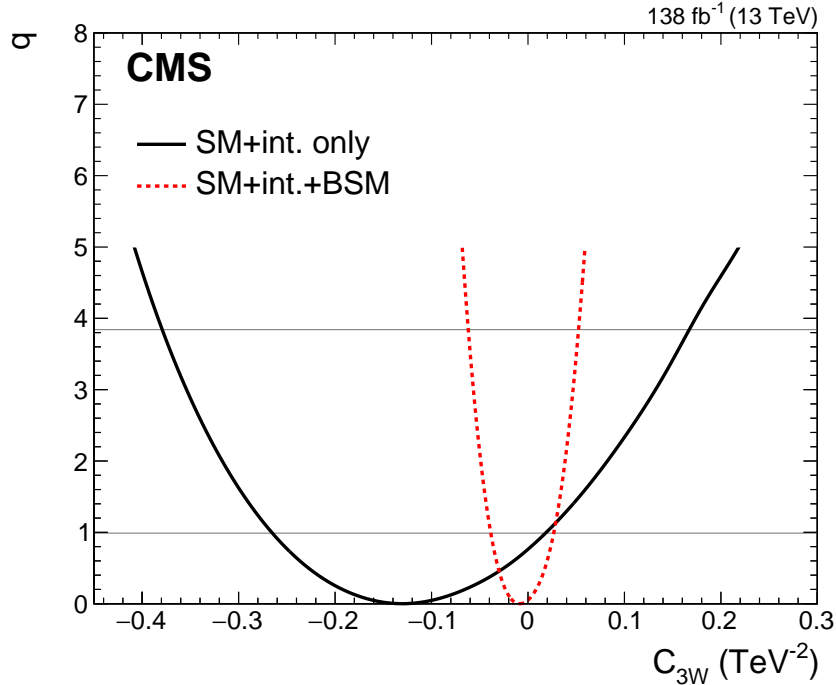


Figure 12: Scans of the profile likelihood test statistic q as a function of C_{3W} , given with and without the pure BSM term by the dashed red and solid black lines, respectively. The full set of p_T^γ and $|\phi_f|$ bins, described in the text, are included for these scans.

Table 4: Best fit values of C_{3W} and corresponding 95% CL confidence intervals as a function of the maximum p_T^γ bin included in the fit.

p_T^γ cutoff (GeV)	Best fit C_{3W} (TeV^{-2})		Observed 95% CL (TeV^{-2})		Expected 95% CL (TeV^{-2})	
	SM+int. only	SM+int.+BSM	SM+int. only	SM+int.+BSM	SM+int. only	SM+int.+BSM
200	-0.86	-0.24	[-2.01, 0.38]	[-0.76, 0.40]	[-1.16, 1.27]	[-0.81, 0.71]
300	-0.25	-0.17	[-0.81, 0.34]	[-0.39, 0.28]	[-0.56, 0.60]	[-0.33, 0.33]
500	-0.13	-0.025	[-0.50, 0.25]	[-0.15, 0.12]	[-0.35, 0.38]	[-0.17, 0.16]
800	-0.20	-0.033	[-0.49, 0.11]	[-0.10, 0.08]	[-0.29, 0.31]	[-0.097, 0.095]
1500	-0.13	-0.009	[-0.38, 0.17]	[-0.062, 0.052]	[-0.27, 0.29]	[-0.066, 0.065]

The constraint including the pure BSM term is similar in value to that of Ref. [6], after accounting for a difference in the normalization of C_{3W} due to the use of an alternative EFT basis. However, the main feature of this result is the ability to constrain C_{3W} when only the interference term is considered. To demonstrate this, the constraints are also determined without the binning in $|\phi_f|$ applied. The same set of p_T^γ bins are used, but the three bins in $|\phi_f|$ are replaced by a single bin integrating over the full $|\phi_f|$ range. The result is shown in Fig. 13 (right), without the inclusion of the pure BSM term. This demonstrates the significant improvement, by up to a factor of ten, that the $|\phi_f|$ binning gives to this constraint.

The interference-only confidence intervals on C_{3W} can be compared with measurements of

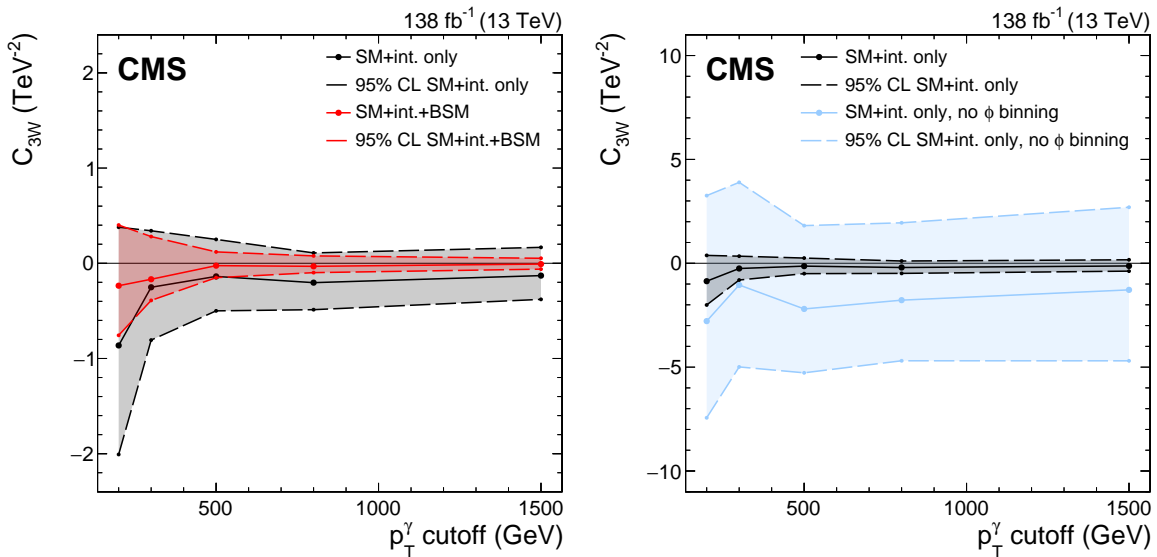


Figure 13: Best-fit values of C_{3W} and the corresponding 95% CL confidence intervals as a function of the maximum p_T^γ bin included in the fit (left). Measurements with and without the pure BSM term are given by the black and red lines, respectively. The limits without the pure BSM term given with and without the binning in $|\phi_f|$ are also shown (right), with black and blue lines, respectively. Please note the different vertical scales; the black lines in both figures correspond to the same limits.

other processes that are sensitive to the \mathcal{O}_{3W} operator. An ATLAS measurement of WW production [83], in which the coefficient is denoted c_W , uses an alternative technique to improve sensitivity to the interference. The presence of an additional high- p_T jet is required, which partially mitigates the helicity suppression effect [13], and gives an interference-only sensitivity that is around a factor of eight lower. The ATLAS measurement of electroweak Z boson production in association with two jets [84] gives comparable sensitivity to our result. It exploits the distribution of the azimuthal angle between the jets, which is sensitive to the interference contribution.

The response matrix R_{ij} for the 2D differential cross section measurement of p_T^γ and $|\phi_f|$ is shown in Fig. 14. Although the migration between p_T^γ bins is small, the migration between $|\phi_f|$ bins is larger, owing both to the limited p_T^{miss} resolution and the fundamental limitations of the method used to reconstruct the neutrino four-momentum via the m_W pole mass constraint.

The resulting cross section measurements are shown in Fig. 15. The measured values are compared with the prediction from the NLO MG5_aMC+PY8 simulation. The correlation matrix is presented in Fig. 16. Unlike the 1D p_T^γ cross section, the correlations between different p_T^γ bins are relatively small, since these measurements at high p_T^γ are much more dominated by the statistical uncertainties. For a given p_T^γ bin the (anti-)correlation between $|\phi_f|$ bins is larger, owing to the migration in the response matrix discussed previously.

10 Summary

This paper has presented an analysis of $W^\pm\gamma$ production in $\sqrt{s} = 13$ TeV proton-proton collisions using data recorded with the CMS detector at the LHC, corresponding to an integrated luminosity of 138 fb^{-1} . Differential cross sections have been measured for several observables and compared with standard model (SM) predictions computed at next-to-leading and next-

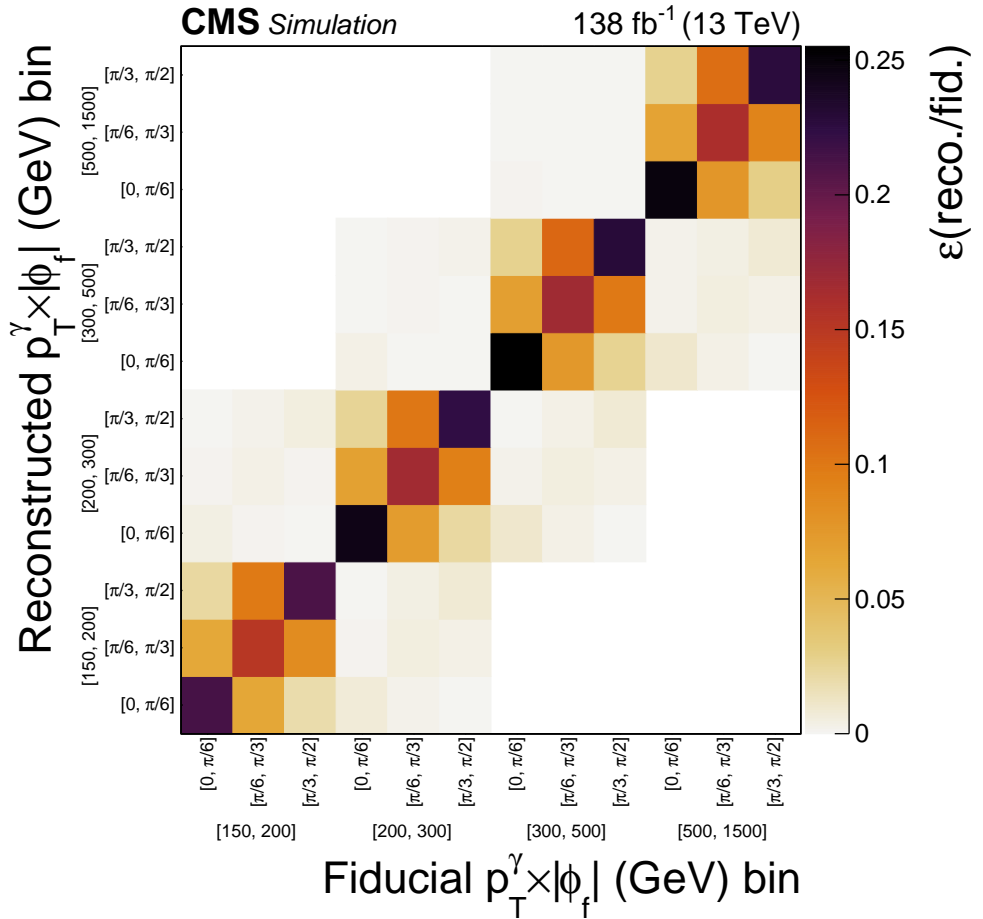


Figure 14: Response matrix for the differential $p_T^\gamma \times |\phi_f|$ cross section measurement. The entry in each bin gives the probability for an event of a given particle-level fiducial bin to be reconstructed in one of the corresponding reconstruction-level bins. The inner labels give the $|\phi_f|$ bin and the outer labels indicate the p_T^γ bin.

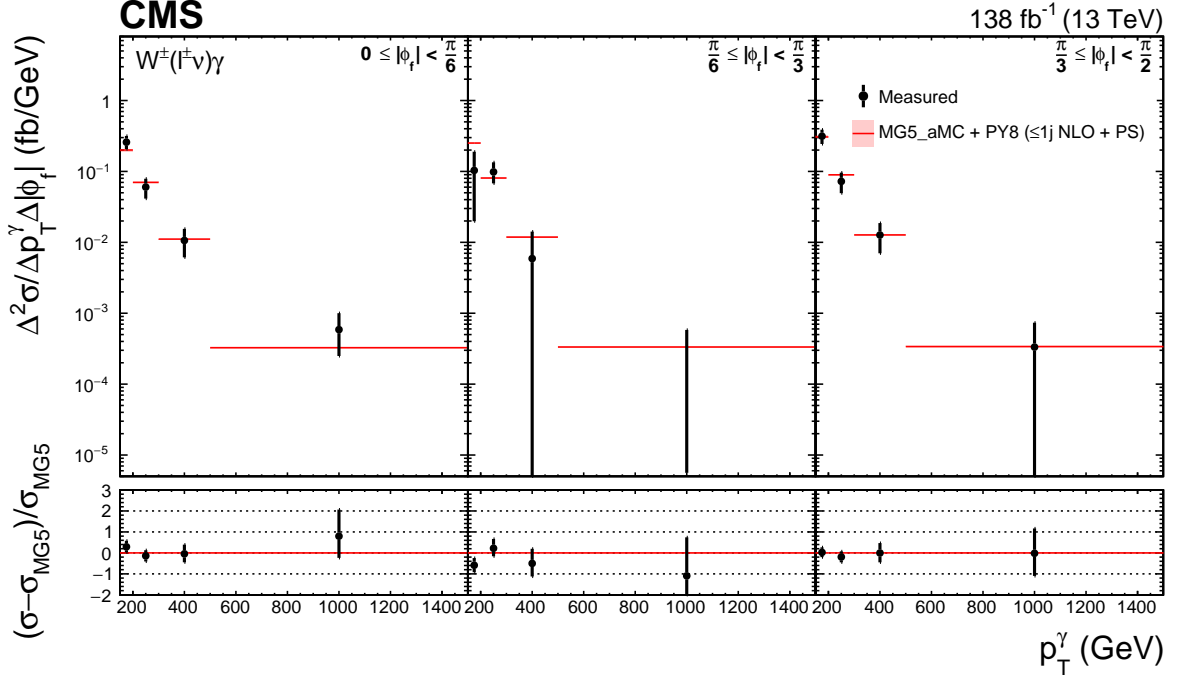


Figure 15: Measured double-differential $p_T \gamma \times |\phi_f|$ cross section and comparison to the MG5_aMC+PY8 NLO prediction. The black vertical bars give the total uncertainty on each measurement. The red shaded bands give the missing higher-order correction uncertainties in the prediction.

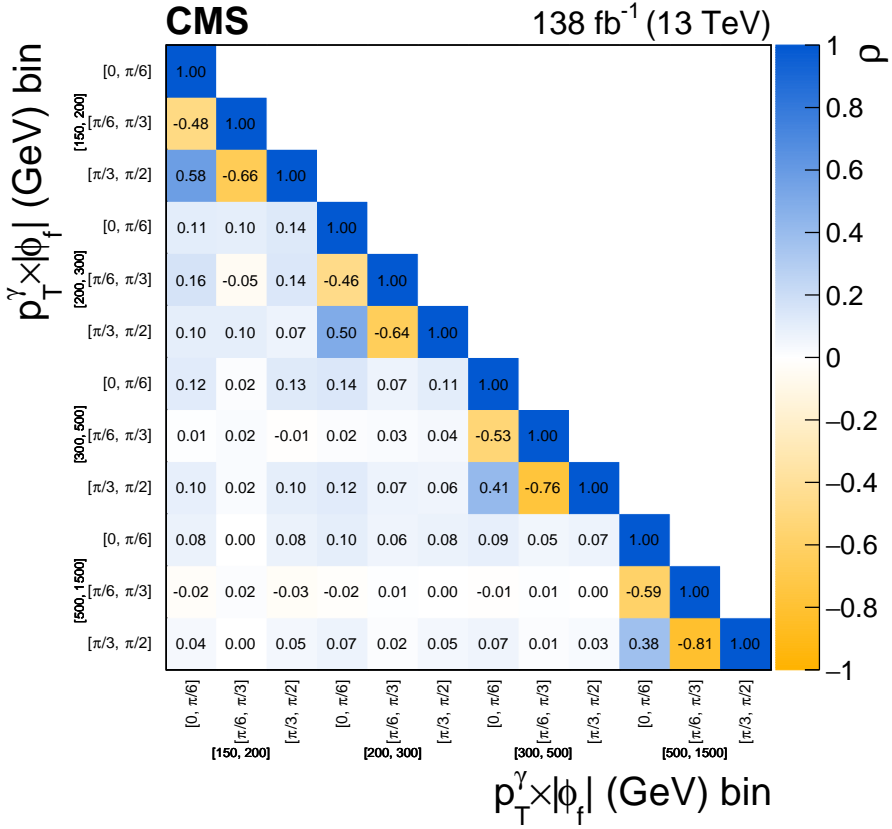


Figure 16: Correlation matrix for the measured $p_T \gamma \times |\phi_f|$ cross sections.

to-next-to-leading orders in perturbative quantum chromodynamics. The radiation amplitude zero effect, caused by interference between $W^\pm\gamma$ production diagrams, has been studied via a measurement of the pseudorapidity difference between the lepton and the photon.

Constraints on the presence of TeV-scale new physics affecting the $WW\gamma$ vertex have been determined using an effective field theory framework. Confidence intervals on the Wilson coefficient C_{3W} , determined at the 95% confidence level, are $[-0.062, 0.052]$ TeV $^{-2}$ with the inclusion of the interference and pure beyond the SM contributions, and $[-0.38, 0.17]$ TeV $^{-2}$ when only the interference is considered. A novel two-dimensional approach is used with the simultaneous measurement of the photon transverse momentum and the azimuthal angle of the charged lepton in a special reference frame. With this method, the sensitivity to the interference between the SM and the \mathcal{O}_{3W} operator is enhanced by up to a factor of ten compared to a measurement using the transverse momentum alone. This improves the validity of the result, as the dependence on the missing higher-order contributions in the EFT expansion is reduced. The technique will also be valuable in the future when sufficiently small values of C_{3W} are probed such that the interference contribution will be dominant.

Acknowledgments

We congratulate our colleagues in the CERN accelerator departments for the excellent performance of the LHC and thank the technical and administrative staffs at CERN and at other CMS institutes for their contributions to the success of the CMS effort. In addition, we gratefully acknowledge the computing centers and personnel of the Worldwide LHC Computing Grid and other centers for delivering so effectively the computing infrastructure essential to our analyses. Finally, we acknowledge the enduring support for the construction and operation of the LHC, the CMS detector, and the supporting computing infrastructure provided by the following funding agencies: BMBWF and FWF (Austria); FNRS and FWO (Belgium); CNPq, CAPES, FAPERJ, FAPERGS, and FAPESP (Brazil); MES and BNSF (Bulgaria); CERN; CAS, MoST, and NSFC (China); MINCIENCIAS (Colombia); MSES and CSF (Croatia); RIF (Cyprus); SENESCYT (Ecuador); MoER, ERC PUT and ERDF (Estonia); Academy of Finland, MEC, and HIP (Finland); CEA and CNRS/IN2P3 (France); BMBF, DFG, and HGF (Germany); GSRI (Greece); NKFIH (Hungary); DAE and DST (India); IPM (Iran); SFI (Ireland); INFN (Italy); MSIP and NRF (Republic of Korea); MES (Latvia); LAS (Lithuania); MOE and UM (Malaysia); BUAP, CINVESTAV, CONACYT, LNS, SEP, and UASLP-FAI (Mexico); MOS (Montenegro); MBIE (New Zealand); PAEC (Pakistan); MSHE and NSC (Poland); FCT (Portugal); JINR (Dubna); MON, RosAtom, RAS, RFBR, and NRC KI (Russia); MESTD (Serbia); SEIDI, CPAN, PCTI, and FEDER (Spain); MOSTR (Sri Lanka); Swiss Funding Agencies (Switzerland); MST (Taipei); ThEPCenter, IPST, STAR, and NSTDA (Thailand); TUBITAK and TAEK (Turkey); NASU (Ukraine); STFC (United Kingdom); DOE and NSF (USA).

Individuals have received support from the Marie-Curie program and the European Research Council and Horizon 2020 Grant, contract Nos. 675440, 724704, 752730, 758316, 765710, 824093, 884104, and COST Action CA16108 (European Union); the Leventis Foundation; the Alfred P. Sloan Foundation; the Alexander von Humboldt Foundation; the Belgian Federal Science Policy Office; the Fonds pour la Formation à la Recherche dans l’Industrie et dans l’Agriculture (FRIA-Belgium); the Agentschap voor Innovatie door Wetenschap en Technologie (IWT-Belgium); the F.R.S.-FNRS and FWO (Belgium) under the “Excellence of Science – EOS” – be.h project n. 30820817; the Beijing Municipal Science & Technology Commission, No. Z191100007219010; the Ministry of Education, Youth and Sports (MEYS) of the Czech Republic; the Deutsche Forschungsgemeinschaft (DFG), under Germany’s Excellence Strat-

egy – EXC 2121 “Quantum Universe” – 390833306, and under project number 400140256 - GRK2497; the Lendület (“Momentum”) Program and the János Bolyai Research Scholarship of the Hungarian Academy of Sciences, the New National Excellence Program ÚNKP, the NKFIA research grants 123842, 123959, 124845, 124850, 125105, 128713, 128786, and 129058 (Hungary); the Council of Science and Industrial Research, India; the Latvian Council of Science; the Ministry of Science and Higher Education and the National Science Center, contracts Opus 2014/15/B/ST2/03998 and 2015/19/B/ST2/02861 (Poland); the Fundação para a Ciência e a Tecnologia, grant CEECIND/01334/2018 (Portugal); the National Priorities Research Program by Qatar National Research Fund; the Ministry of Science and Higher Education, projects no. 14.W03.31.0026 and no. FSWW-2020-0008, and the Russian Foundation for Basic Research, project No.19-42-703014 (Russia); the Programa Estatal de Fomento de la Investigación Científica y Técnica de Excelencia María de Maeztu, grant MDM-2015-0509 and the Programa Severo Ochoa del Principado de Asturias; the Stavros Niarchos Foundation (Greece); the Rachadapisek Sompot Fund for Postdoctoral Fellowship, Chulalongkorn University and the Chulalongkorn Academic into Its 2nd Century Project Advancement Project (Thailand); the Kavli Foundation; the Nvidia Corporation; the SuperMicro Corporation; the Welch Foundation, contract C-1845; and the Weston Havens Foundation (USA).

References

- [1] CDF Collaboration, “Measurement of $W\gamma$ and $Z\gamma$ production in $p\bar{p}$ collisions at $\sqrt{s} = 1.96$ TeV”, *Phys. Rev. Lett.* **94** (2005) 041803,
 $\text{doi:10.1103/PhysRevLett.94.041803}$, arXiv:hep-ex/0410008.
- [2] D0 Collaboration, “Measurement of the $p\bar{p} \rightarrow W\gamma + X$ cross section at $\sqrt{s} = 1.96$ TeV and $WW\gamma$ anomalous coupling limits”, *Phys. Rev. D* **71** (2005) 091108,
 $\text{doi:10.1103/PhysRevD.71.091108}$, arXiv:hep-ex/0503048.
- [3] D0 Collaboration, “First study of the radiation-amplitude zero in $W\gamma$ production and limits on anomalous $WW\gamma$ couplings at $\sqrt{s} = 1.96$ TeV”, *Phys. Rev. Lett.* **100** (2008) 241805, $\text{doi:10.1103/PhysRevLett.100.241805}$, arXiv:0803.0030.
- [4] CMS Collaboration, “Measurement of the $W\gamma$ and $Z\gamma$ inclusive cross sections in pp collisions at $\sqrt{s} = 7$ TeV and limits on anomalous triple gauge boson couplings”, *Phys. Rev. D* **89** (2014) 092005, $\text{doi:10.1103/PhysRevD.89.092005}$, arXiv:1308.6832.
- [5] ATLAS Collaboration, “Measurements of $W\gamma$ and $Z\gamma$ production in pp collisions at $\sqrt{s} = 7$ TeV with the ATLAS detector at the LHC”, *Phys. Rev. D* **87** (2013) 112003,
 $\text{doi:10.1103/PhysRevD.87.112003}$, arXiv:1302.1283. [Erratum:
 $\text{doi:10.1103/PhysRevD.91.119901}$].
- [6] CMS Collaboration, “Measurement of the $W\gamma$ production cross section in proton-proton collisions at $\sqrt{s} = 13$ TeV and constraints on effective field theory coefficients”, *Phys. Rev. Lett.* **126** (2021) 252002, $\text{doi:10.1103/PhysRevLett.126.252002}$, arXiv:2102.02283.
- [7] K. O. Mikaelian, M. A. Samuel, and D. Sahdev, “Magnetic moment of weak bosons produced in pp and $p\bar{p}$ collisions”, *Phys. Rev. Lett.* **43** (1979) 746,
 $\text{doi:10.1103/PhysRevLett.43.746}$.

- [8] C. J. Goebel, F. Halzen, and J. P. Leveille, “Angular zeros of Brown, Mikaelian, Sahdev, and Samuel and the factorization of tree amplitudes in gauge theories”, *Phys. Rev. D* **23** (1981) 2682, doi:[10.1103/PhysRevD.23.2682](https://doi.org/10.1103/PhysRevD.23.2682).
- [9] S. J. Brodsky and R. W. Brown, “Zeros in amplitudes: Gauge theory and radiation interference”, *Phys. Rev. Lett.* **49** (1982) 966, doi:[10.1103/PhysRevLett.49.966](https://doi.org/10.1103/PhysRevLett.49.966).
- [10] R. W. Brown, K. L. Kowalski, and S. J. Brodsky, “Classical radiation zeros in gauge theory amplitudes”, *Phys. Rev. D* **28** (1983) 624, doi:[10.1103/PhysRevD.28.624](https://doi.org/10.1103/PhysRevD.28.624). [Addendum: doi:[10.1103/PhysRevD.29.2100](https://doi.org/10.1103/PhysRevD.29.2100)].
- [11] U. Baur, S. Errede, and G. L. Landsberg, “Rapidity correlations in $W\gamma$ production at hadron colliders”, *Phys. Rev. D* **50** (1994) 1917, doi:[10.1103/PhysRevD.50.1917](https://doi.org/10.1103/PhysRevD.50.1917), arXiv:[hep-ph/9402282](https://arxiv.org/abs/hep-ph/9402282).
- [12] G. Panico, F. Riva, and A. Wulzer, “Diboson interference resurrection”, *Phys. Lett. B* **776** (2018) 473, doi:[10.1016/j.physletb.2017.11.068](https://doi.org/10.1016/j.physletb.2017.11.068), arXiv:[1708.07823](https://arxiv.org/abs/1708.07823).
- [13] A. Azatov, J. Elias-Miró, Y. Reyimuaji, and E. Venturini, “Novel measurements of anomalous triple gauge couplings for the LHC”, *JHEP* **10** (2017) 027, doi:[10.1007/JHEP10\(2017\)027](https://doi.org/10.1007/JHEP10(2017)027), arXiv:[1707.08060](https://arxiv.org/abs/1707.08060).
- [14] S. Weinberg, “Baryon- and lepton-nonconserving processes”, *Phys. Rev. Lett.* **43** (1979) 1566, doi:[10.1103/PhysRevLett.43.1566](https://doi.org/10.1103/PhysRevLett.43.1566).
- [15] D. Liu, A. Pomarol, R. Rattazzi, and F. Riva, “Patterns of strong coupling for LHC searches”, *JHEP* **11** (2016) 141, doi:[10.1007/JHEP11\(2016\)141](https://doi.org/10.1007/JHEP11(2016)141), arXiv:[1603.03064](https://arxiv.org/abs/1603.03064).
- [16] D. Marzocca et al., “BSM benchmarks for effective field theories in Higgs and electroweak physics”, 2020. arXiv:[2009.01249](https://arxiv.org/abs/2009.01249).
- [17] B. Grzadkowski, M. Iskrzyński, M. Misiak, and J. Rosiek, “Dimension-six terms in the standard model Lagrangian”, *JHEP* **10** (2010) 085, doi:[10.1007/JHEP10\(2010\)085](https://doi.org/10.1007/JHEP10(2010)085), arXiv:[1008.4884](https://arxiv.org/abs/1008.4884).
- [18] A. Azatov, R. Contino, C. S. Machado, and F. Riva, “Helicity selection rules and noninterference for BSM amplitudes”, *Phys. Rev. D* **95** (2017) 065014, doi:[10.1103/PhysRevD.95.065014](https://doi.org/10.1103/PhysRevD.95.065014), arXiv:[1607.05236](https://arxiv.org/abs/1607.05236).
- [19] A. Azatov, D. Barducci, and E. Venturini, “Precision diboson measurements at hadron colliders”, *JHEP* **04** (2019) 075, doi:[10.1007/JHEP04\(2019\)075](https://doi.org/10.1007/JHEP04(2019)075), arXiv:[1901.04821](https://arxiv.org/abs/1901.04821).
- [20] J. Alwall et al., “Comparative study of various algorithms for the merging of parton showers and matrix elements in hadronic collisions”, *Eur. Phys. J. C* **53** (2008) 473, doi:[10.1140/epjc/s10052-007-0490-5](https://doi.org/10.1140/epjc/s10052-007-0490-5), arXiv:[0706.2569](https://arxiv.org/abs/0706.2569).
- [21] CMS Collaboration, “Performance of photon reconstruction and identification with the CMS detector in proton-proton collisions at $\sqrt{s} = 8$ TeV”, *JINST* **10** (2015) P08010, doi:[10.1088/1748-0221/10/08/P08010](https://doi.org/10.1088/1748-0221/10/08/P08010), arXiv:[1502.02702](https://arxiv.org/abs/1502.02702).
- [22] CMS Collaboration, “Performance of electron reconstruction and selection with the CMS detector in proton-proton collisions at $\sqrt{s} = 8$ TeV”, *JINST* **10** (2015) P06005, doi:[10.1088/1748-0221/10/06/P06005](https://doi.org/10.1088/1748-0221/10/06/P06005), arXiv:[1502.02701](https://arxiv.org/abs/1502.02701).

- [23] CMS Collaboration, “Performance of the CMS muon detector and muon reconstruction with proton-proton collisions at $\sqrt{s} = 13$ TeV”, *JINST* **13** (2018) P06015, doi:10.1088/1748-0221/13/06/P06015, arXiv:1804.04528.
- [24] CMS Collaboration, “Performance of the CMS Level-1 trigger in proton-proton collisions at $\sqrt{s} = 13$ TeV”, *JINST* **15** (2020) P10017, doi:10.1088/1748-0221/15/10/P10017, arXiv:2006.10165.
- [25] CMS Collaboration, “The CMS trigger system”, *JINST* **12** (2017) P01020, doi:10.1088/1748-0221/12/01/P01020, arXiv:1609.02366.
- [26] CMS Collaboration, “The CMS experiment at the CERN LHC”, *JINST* **3** (2008) S08004, doi:10.1088/1748-0221/3/08/S08004.
- [27] J. Alwall et al., “The automated computation of tree-level and next-to-leading order differential cross sections, and their matching to parton shower simulations”, *JHEP* **07** (2014) 079, doi:10.1007/JHEP07(2014)079, arXiv:1405.0301.
- [28] P. Nason, “A new method for combining NLO QCD with shower Monte Carlo algorithms”, *JHEP* **11** (2004) 040, doi:10.1088/1126-6708/2004/11/040, arXiv:hep-ph/0409146.
- [29] S. Frixione, P. Nason, and C. Oleari, “Matching NLO QCD computations with parton shower simulations: the POWHEG method”, *JHEP* **11** (2007) 070, doi:10.1088/1126-6708/2007/11/070, arXiv:0709.2092.
- [30] S. Alioli, P. Nason, C. Oleari, and E. Re, “A general framework for implementing NLO calculations in shower Monte Carlo programs: the POWHEG BOX”, *JHEP* **06** (2010) 043, doi:10.1007/JHEP06(2010)043, arXiv:1002.2581.
- [31] S. Frixione, P. Nason, and G. Ridolfi, “A positive-weight next-to-leading-order Monte Carlo for heavy flavour hadroproduction”, *JHEP* **09** (2007) 126, doi:10.1088/1126-6708/2007/09/126, arXiv:0707.3088.
- [32] R. Frederix, E. Re, and P. Torrielli, “Single-top t-channel hadroproduction in the four-flavour scheme with POWHEG and aMC@NLO”, *JHEP* **09** (2012) 130, doi:10.1007/JHEP09(2012)130, arXiv:1207.5391.
- [33] E. Re, “Single-top Wt-channel production matched with parton showers using the POWHEG method”, *Eur. Phys. J. C* **71** (2011) 1547, doi:10.1140/epjc/s10052-011-1547-z, arXiv:1009.2450.
- [34] O. Mattelaer, “On the maximal use of Monte Carlo samples: re-weighting events at NLO accuracy”, *Eur. Phys. J. C* **76** (2016) 674, doi:10.1140/epjc/s10052-016-4533-7, arXiv:1607.00763.
- [35] I. Brivio, Y. Jiang, and M. Trott, “The SMEFTsim package, theory and tools”, *JHEP* **12** (2017) 070, doi:10.1007/JHEP12(2017)070, arXiv:1709.06492.
- [36] I. Brivio, “SMEFTsim 3.0 — a practical guide”, *JHEP* **04** (2021) 073, doi:10.1007/JHEP04(2021)073, arXiv:2012.11343.
- [37] NNPDF Collaboration, “Parton distributions from high-precision collider data”, *Eur. Phys. J. C* **77** (2017) 663, doi:10.1140/epjc/s10052-017-5199-5, arXiv:1706.00428.

- [38] NNPDF Collaboration, “Parton distributions for the LHC Run II”, *JHEP* **04** (2015) 040, doi:[10.1007/JHEP04\(2015\)040](https://doi.org/10.1007/JHEP04(2015)040), arXiv:[1410.8849](https://arxiv.org/abs/1410.8849).
- [39] T. Sjöstrand et al., “An introduction to PYTHIA 8.2”, *Comput. Phys. Commun.* **191** (2015) 159, doi:[10.1016/j.cpc.2015.01.024](https://doi.org/10.1016/j.cpc.2015.01.024), arXiv:[1410.3012](https://arxiv.org/abs/1410.3012).
- [40] CMS Collaboration, “Event generator tunes obtained from underlying event and multiparton scattering measurements”, *Eur. Phys. J. C* **76** (2016) 155, doi:[10.1140/epjc/s10052-016-3988-x](https://doi.org/10.1140/epjc/s10052-016-3988-x), arXiv:[1512.00815](https://arxiv.org/abs/1512.00815).
- [41] CMS Collaboration, “Investigations of the impact of the parton shower tuning in Pythia 8 in the modelling of $t\bar{t}$ at $\sqrt{s} = 8$ and 13 TeV”, CMS Physics Analysis Summary CMS-PAS-TOP-16-021, 2016.
- [42] CMS Collaboration, “Extraction and validation of a new set of CMS PYTHIA8 tunes from underlying-event measurements”, *Eur. Phys. J. C* **80** (2020) 4, doi:[10.1140/epjc/s10052-019-7499-4](https://doi.org/10.1140/epjc/s10052-019-7499-4), arXiv:[1903.12179](https://arxiv.org/abs/1903.12179).
- [43] GEANT4 Collaboration, “GEANT4—a simulation toolkit”, *Nucl. Instrum. Meth. A* **506** (2003) 250, doi:[10.1016/S0168-9002\(03\)01368-8](https://doi.org/10.1016/S0168-9002(03)01368-8).
- [44] M. Cacciari, G. P. Salam, and G. Soyez, “The anti- k_T jet clustering algorithm”, *JHEP* **04** (2008) 063, doi:[10.1088/1126-6708/2008/04/063](https://doi.org/10.1088/1126-6708/2008/04/063), arXiv:[0802.1189](https://arxiv.org/abs/0802.1189).
- [45] M. Cacciari, G. P. Salam, and G. Soyez, “FastJet user manual”, *Eur. Phys. J. C* **72** (2012) 1896, doi:[10.1140/epjc/s10052-012-1896-2](https://doi.org/10.1140/epjc/s10052-012-1896-2), arXiv:[1111.6097](https://arxiv.org/abs/1111.6097).
- [46] CMS Collaboration, “Particle-flow reconstruction and global event description with the CMS detector”, *JINST* **12** (2017) P10003, doi:[10.1088/1748-0221/12/10/P10003](https://doi.org/10.1088/1748-0221/12/10/P10003), arXiv:[1706.04965](https://arxiv.org/abs/1706.04965).
- [47] CMS Collaboration, “Jet energy scale and resolution in the CMS experiment in pp collisions at 8 TeV”, *JINST* **12** (2017) P02014, doi:[10.1088/1748-0221/12/02/P02014](https://doi.org/10.1088/1748-0221/12/02/P02014), arXiv:[1607.03663](https://arxiv.org/abs/1607.03663).
- [48] CMS Collaboration, “Electron and photon reconstruction and identification with the CMS experiment at the CERN LHC”, *JINST* **16** (2021) P05014, doi:[10.1088/1748-0221/16/05/p05014](https://doi.org/10.1088/1748-0221/16/05/p05014), arXiv:[2012.06888](https://arxiv.org/abs/2012.06888).
- [49] CMS Collaboration, “Measurements of inclusive W and Z cross sections in pp collisions at $\sqrt{s} = 7$ TeV”, *JHEP* **01** (2011) 080, doi:[10.1007/JHEP01\(2011\)080](https://doi.org/10.1007/JHEP01(2011)080), arXiv:[1012.2466](https://arxiv.org/abs/1012.2466).
- [50] A. Bodek et al., “Extracting muon momentum scale corrections for hadron collider experiments”, *Eur. Phys. J. C* **72** (2012) 2194, doi:[10.1140/epjc/s10052-012-2194-8](https://doi.org/10.1140/epjc/s10052-012-2194-8), arXiv:[1208.3710](https://arxiv.org/abs/1208.3710).
- [51] CMS Collaboration, “Performance of missing transverse momentum reconstruction in proton-proton collisions at $\sqrt{s} = 13$ TeV using the CMS detector”, *JINST* **14** (2019) P07004, doi:[10.1088/1748-0221/14/07/P07004](https://doi.org/10.1088/1748-0221/14/07/P07004), arXiv:[1903.06078](https://arxiv.org/abs/1903.06078).
- [52] D. Bertolini, P. Harris, M. Low, and N. Tran, “Pileup per particle identification”, *JHEP* **10** (2014) 059, doi:[10.1007/JHEP10\(2014\)059](https://doi.org/10.1007/JHEP10(2014)059), arXiv:[1407.6013](https://arxiv.org/abs/1407.6013).

- [53] CMS Collaboration, “Precision luminosity measurement in proton-proton collisions at $\sqrt{s} = 13$ TeV in 2015 and 2016 at CMS”, *Eur. Phys. J. C* **81** (2021) 800, doi:10.1140/epjc/s10052-021-09538-2, arXiv:2104.01927.
- [54] CMS Collaboration, “CMS luminosity measurement for the 2017 data-taking period at $\sqrt{s} = 13$ TeV”, CMS Physics Analysis Summary CMS-PAS-LUM-17-004, 2018.
- [55] CMS Collaboration, “CMS luminosity measurement for the 2018 data-taking period at $\sqrt{s} = 13$ TeV”, CMS Physics Analysis Summary CMS-PAS-LUM-18-002, 2019.
- [56] CMS Collaboration, “Measurement of the inelastic proton-proton cross section at $\sqrt{s} = 13$ TeV”, *JHEP* **07** (2018) 161, doi:10.1007/JHEP07(2018)161, arXiv:1802.02613.
- [57] R. J. Barlow and C. Beeston, “Fitting using finite Monte Carlo samples”, *Comput. Phys. Commun.* **77** (1993) 219, doi:10.1016/0010-4655(93)90005-W.
- [58] J. Butterworth et al., “PDF4LHC recommendations for LHC Run II”, *J. Phys. G* **43** (2016) 023001, doi:10.1088/0954-3899/43/2/023001, arXiv:1510.03865.
- [59] I. W. Stewart and F. J. Tackmann, “Theory uncertainties for Higgs mass and other searches using jet bins”, *Phys. Rev. D* **85** (2012) 034011, doi:10.1103/PhysRevD.85.034011, arXiv:1107.2117.
- [60] The ATLAS Collaboration, The CMS Collaboration, The LHC Higgs Combination Group, “Procedure for the LHC Higgs boson search combination in Summer 2011”, Technical Report CMS-NOTE-2011-005, ATL-PHYS-PUB-2011-11, 2011.
- [61] ATLAS and CMS Collaborations, “Measurements of the Higgs boson production and decay rates and constraints on its couplings from a combined ATLAS and CMS analysis of the LHC pp collision data at $\sqrt{s} = 7$ and 8 TeV”, *JHEP* **08** (2016) 45, doi:10.1007/JHEP08(2016)045, arXiv:1606.02266.
- [62] W. Verkerke and D. P. Kirkby, “The RooFit toolkit for data modeling”, in *Proceedings of the 13th International Conference for Computing in High-Energy and Nuclear Physics (CHEP03)*. 2003. arXiv:physics/0306116. [eConf C0303241, MOLT007].
- [63] L. Moneta et al., “The RooStats project”, in *13th International Workshop on Advanced Computing and Analysis Techniques in Physics Research (ACAT2010)*. 2010. arXiv:1009.1003. [PoS(ACAT2010)057]. doi:10.22323/1.093.0057.
- [64] G. Cowan, K. Cranmer, E. Gross, and O. Vitells, “Asymptotic formulae for likelihood-based tests of new physics”, *Eur. Phys. J. C* **71** (2011) 1554, doi:10.1140/epjc/s10052-011-1554-0, arXiv:1007.1727. [Erratum: doi:10.1140/epjc/s10052-013-2501-z].
- [65] HEPData record for this analysis, 2021. doi:10.17182/hepdata.115354.
- [66] S. Frixione, “Isolated photons in perturbative QCD”, *Phys. Lett. B* **429** (1998) 369, doi:10.1016/S0370-2693(98)00454-7, arXiv:hep-ph/9801442.
- [67] M. Grazzini, S. Kallweit, and M. Wiesemann, “Fully differential NNLO computations with MATRIX”, *Eur. Phys. J. C* **78** (2018) 537, doi:10.1140/epjc/s10052-018-5771-7, arXiv:1711.06631.

- [68] M. Grazzini, S. Kallweit, and D. Rathlev, “ $W\gamma$ and $Z\gamma$ production at the LHC in NNLO QCD”, *JHEP* **07** (2015) 085, doi:10.1007/JHEP07(2015)085, arXiv:1504.01330.
- [69] J. M. Campbell, G. De Laurentis, R. K. Ellis, and S. Seth, “The $pp \rightarrow W(\rightarrow l\nu) + \gamma$ process at next-to-next-to-leading order”, *JHEP* **07** (2021) 079, doi:10.1007/JHEP07(2021)079, arXiv:2105.00954.
- [70] J. M. Campbell, R. K. Ellis, and C. Williams, “Vector boson pair production at the LHC”, *JHEP* **07** (2011) 018, doi:10.1007/JHEP07(2011)018, arXiv:1105.0020.
- [71] T. Cridge, M. A. Lim, and R. Nagar, “ $W\gamma$ production at NNLO+PS accuracy in GENEVA”, *Phys. Lett. B* **826** (2022) 136918, doi:10.1016/j.physletb.2022.136918, arXiv:2105.13214.
- [72] S. Alioli et al., “Combining higher-order resummation with multiple NLO calculations and parton showers in GENEVA”, *JHEP* **09** (2013) 120, doi:10.1007/JHEP09(2013)120, arXiv:1211.7049.
- [73] S. Alioli et al., “Drell-Yan production at NNLL'+NNLO matched to parton showers”, *Phys. Rev. D* **92** (2015) 094020, doi:10.1103/PhysRevD.92.094020, arXiv:1508.01475.
- [74] S. Alioli et al., “Matching NNLO predictions to parton showers using N^3LL color-singlet transverse momentum resummation in GENEVA”, *Phys. Rev. D* **104** (2021) 094020, doi:10.1103/PhysRevD.104.094020, arXiv:2102.08390.
- [75] S. Catani et al., “Vector boson production at hadron colliders: hard-collinear coefficients at the NNLO”, *Eur. Phys. J. C* **72** (2012) 2195, doi:10.1140/epjc/s10052-012-2195-7, arXiv:1209.0158.
- [76] S. Catani and M. Grazzini, “Next-to-next-to-leading-order subtraction formalism in hadron collisions and its application to Higgs-boson production at the Large Hadron Collider”, *Phys. Rev. Lett.* **98** (2007) 222002, doi:10.1103/PhysRevLett.98.222002, arXiv:hep-ph/0703012.
- [77] F. Cascioli, P. Maierhöfer, and S. Pozzorini, “Scattering amplitudes with Open Loops”, *Phys. Rev. Lett.* **108** (2012) 111601, doi:10.1103/PhysRevLett.108.111601, arXiv:1111.5206.
- [78] A. Denner, S. Dittmaier, and L. Hofer, “Collier: a fortran-based complex one-loop library in extended regularizations”, *Comput. Phys. Commun.* **212** (2017) 220, doi:10.1016/j.cpc.2016.10.013, arXiv:1604.06792.
- [79] T. Gehrmann and L. Tancredi, “Two-loop QCD helicity amplitudes for $q\bar{q} \rightarrow W^\pm\gamma$ and $q\bar{q} \rightarrow Z^0\gamma$ ”, *JHEP* **02** (2012) 004, doi:10.1007/JHEP02(2012)004, arXiv:1112.1531.
- [80] A. Denner, S. Dittmaier, M. Hecht, and C. Pasold, “NLO QCD and electroweak corrections to $W+\gamma$ production with leptonic W-boson decays”, *JHEP* **04** (2015) 018, doi:10.1007/JHEP04(2015)018, arXiv:1412.7421.
- [81] R. M. Capdevilla, R. Harnik, and A. Martin, “The radiation valley and exotic resonances in $W\gamma$ production at the LHC”, *JHEP* **03** (2020) 117, doi:10.1007/JHEP03(2020)117, arXiv:1912.08234.

- [82] R. Contino et al., “On the validity of the effective field theory approach to SM precision tests”, *JHEP* **07** (2016) 144, doi:10.1007/JHEP07(2016)144, arXiv:1604.06444.
- [83] ATLAS Collaboration, “Measurements of $W^+W^- + \geq 1$ jet production cross-sections in pp collisions at $\sqrt{s} = 13$ TeV with the ATLAS detector”, *JHEP* **06** (2021) 003, doi:10.1007/JHEP06(2021)003, arXiv:2103.10319.
- [84] ATLAS Collaboration, “Differential cross-section measurements for the electroweak production of dijets in association with a Z boson in proton–proton collisions at ATLAS”, *Eur. Phys. J. C* **81** (2021) 163, doi:10.1140/epjc/s10052-020-08734-w, arXiv:2006.15458.

A The CMS Collaboration

Yerevan Physics Institute, Yerevan, Armenia

A. Tumasyan

Institut für Hochenergiephysik, Vienna, Austria

W. Adam , J.W. Andrejkovic, T. Bergauer , S. Chatterjee , M. Dragicevic , A. Escalante Del Valle , R. Frühwirth¹, M. Jeitler¹ , N. Krammer, L. Lechner , D. Liko, I. Mikulec, P. Paulitsch, F.M. Pitters, J. Schieck¹ , R. Schöfbeck , M. Spanring , S. Templ , W. Waltenberger , C.-E. Wulz¹ 

Institute for Nuclear Problems, Minsk, Belarus

V. Chekhovsky, A. Litomin, V. Makarenko 

Universiteit Antwerpen, Antwerpen, Belgium

M.R. Darwish², E.A. De Wolf, T. Janssen , T. Kello³, A. Lelek , H. Rejeb Sfar, P. Van Mechelen , S. Van Putte, N. Van Remortel 

Vrije Universiteit Brussel, Brussel, Belgium

F. Blekman , E.S. Bols , J. D'Hondt , J. De Clercq , M. Delcourt, H. El Faham , S. Lowette , S. Moortgat , A. Morton , D. Müller , A.R. Sahasransu , S. Tavernier , W. Van Doninck, P. Van Mulders

Université Libre de Bruxelles, Bruxelles, Belgium

D. Beghin, B. Bilin , B. Clerbaux , G. De Lentdecker, L. Favart , A. Grebenyuk, A.K. Kalsi , K. Lee, M. Mahdavikhorrami, I. Makarenko , L. Moureaux , L. Pétré, A. Popov , N. Postiau, E. Starling , L. Thomas , M. Vanden Bemden, C. Vander Velde , P. Vanlaer , D. Vannerom , L. Wezenbeek

Ghent University, Ghent, Belgium

T. Cornelis , D. Dobur, J. Knolle , L. Lambrecht, G. Mestdach, M. Niedziela , C. Roskas, A. Samalan, K. Skovpen , M. Tytgat , W. Verbeke, B. Vermassen, M. Vit

Université Catholique de Louvain, Louvain-la-Neuve, Belgium

A. Bethani , G. Bruno, F. Bury , C. Caputo , P. David , C. Delaere , I.S. Donertas , A. Giammanco , K. Jaffel, Sa. Jain , V. Lemaitre, K. Mondal , J. Prisciandaro, A. Taliercio, M. Teklishyn , T.T. Tran, P. Vischia , S. Wertz 

Centro Brasileiro de Pesquisas Fisicas, Rio de Janeiro, Brazil

G.A. Alves , C. Hensel, A. Moraes 

Universidade do Estado do Rio de Janeiro, Rio de Janeiro, Brazil

W.L. Aldá Júnior , M. Alves Gallo Pereira , M. Barroso Ferreira Filho, H. BRANDAO MALBOUSSON, W. Carvalho , J. Chinellato⁴, E.M. Da Costa , G.G. Da Silveira⁵ , D. De Jesus Damiao , S. Fonseca De Souza , D. Matos Figueiredo, C. Mora Herrera , K. Mota Amarilo, L. Mundim , H. Nogima, P. Rebello Teles , A. Santoro, S.M. Silva Do Amaral , A. Sznajder , M. Thiel, F. Torres Da Silva De Araujo , A. Vilela Pereira 

Universidade Estadual Paulista (a), Universidade Federal do ABC (b), São Paulo, Brazil

C.A. Bernardes⁵ , L. Calligaris , T.R. Fernandez Perez Tomei , E.M. Gregores , D.S. Lemos , P.G. Mercadante , S.F. Novaes , Sandra S. Padula 

Institute for Nuclear Research and Nuclear Energy, Bulgarian Academy of Sciences, Sofia, Bulgaria

A. Aleksandrov, G. Antchev , R. Hadjiiska, P. Iaydjiev, M. Misheva, M. Rodozov, M. Shopova,

G. Sultanov

University of Sofia, Sofia, Bulgaria

A. Dimitrov, T. Ivanov, L. Litov , B. Pavlov, P. Petkov, A. Petrov

Beihang University, Beijing, China

T. Cheng , Q. Guo, T. Javaid⁶, M. Mittal, H. Wang, L. Yuan

Department of Physics, Tsinghua University, Beijing, China

M. Ahmad , G. Bauer, C. Dozen⁷ , Z. Hu , J. Martins⁸ , Y. Wang, K. Yi^{9,10}

Institute of High Energy Physics, Beijing, China

E. Chapon , G.M. Chen⁶ , H.S. Chen⁶ , M. Chen , F. Iemmi, A. Kapoor , D. Leggat, H. Liao, Z.-A. Liu⁶ , V. Milosevic , F. Monti , R. Sharma , J. Tao , J. Thomas-Wilsker, J. Wang , H. Zhang , S. Zhang⁶, J. Zhao 

State Key Laboratory of Nuclear Physics and Technology, Peking University, Beijing, China

A. Agapitos, Y. Ban, C. Chen, Q. Huang, A. Levin , Q. Li , X. Lyu, Y. Mao, S.J. Qian, D. Wang , Q. Wang , J. Xiao

Sun Yat-Sen University, Guangzhou, China

M. Lu, Z. You 

Institute of Modern Physics and Key Laboratory of Nuclear Physics and Ion-beam Application (MOE) - Fudan University, Shanghai, China

X. Gao³, H. Okawa 

Zhejiang University, Hangzhou, China, Zhejiang, China

Z. Lin , M. Xiao 

Universidad de Los Andes, Bogota, Colombia

C. Avila , A. Cabrera , C. Florez , J. Fraga, A. Sarkar , M.A. Segura Delgado

Universidad de Antioquia, Medellin, Colombia

J. Mejia Guisao, F. Ramirez, J.D. Ruiz Alvarez , C.A. Salazar Gonzalez 

University of Split, Faculty of Electrical Engineering, Mechanical Engineering and Naval Architecture, Split, Croatia

D. Giljanovic, N. Godinovic , D. Lelas , I. Puljak 

University of Split, Faculty of Science, Split, Croatia

Z. Antunovic, M. Kovac, T. Sculac 

Institute Rudjer Boskovic, Zagreb, Croatia

V. Brigljevic , D. Ferencek , D. Majumder , M. Roguljic, A. Starodumov¹¹ , T. Susa 

University of Cyprus, Nicosia, Cyprus

A. Attikis , K. Christoforou, E. Erodotou, A. Ioannou, G. Kole , M. Kolosova, S. Konstantinou, J. Mousa , C. Nicolaou, F. Ptochos , P.A. Razis, H. Rykaczewski, H. Saka 

Charles University, Prague, Czech Republic

M. Finger¹², M. Finger Jr.¹² , A. Kveton

Escuela Politecnica Nacional, Quito, Ecuador

E. Ayala

Universidad San Francisco de Quito, Quito, Ecuador

E. Carrera Jarrin 

Academy of Scientific Research and Technology of the Arab Republic of Egypt, Egyptian Network of High Energy Physics, Cairo, Egypt

A.A. Abdelalim^{13,14} , S. Abu Zeid¹⁵ 

Center for High Energy Physics (CHEP-FU), Fayoum University, El-Fayoum, Egypt

M.A. Mahmoud , Y. Mohammed 

National Institute of Chemical Physics and Biophysics, Tallinn, Estonia

S. Bhowmik , R.K. Dewanjee , K. Ehataht, M. Kadastik, S. Nandan, C. Nielsen, J. Pata, M. Raidal , L. Tani, C. Veelken

Department of Physics, University of Helsinki, Helsinki, Finland

P. Eerola , L. Forthomme , H. Kirschenmann , K. Osterberg , M. Voutilainen 

Helsinki Institute of Physics, Helsinki, Finland

S. Bharthuar, E. Brücke , F. Garcia , J. Havukainen , M.S. Kim , R. Kinnunen, T. Lampén, K. Lassila-Perini , S. Lehti , T. Lindén, M. Lotti, L. Martikainen, M. Myllymäki, J. Ott , H. Siikonen, E. Tuominen , J. Tuomiemi

Lappeenranta University of Technology, Lappeenranta, Finland

P. Luukka , H. Petrow, T. Tuuva

IRFU, CEA, Université Paris-Saclay, Gif-sur-Yvette, France

C. Amendola , M. Besancon, F. Couderc , M. Dejardin, D. Denegri, J.L. Faure, F. Ferri , S. Ganjour, A. Givernaud, P. Gras, G. Hamel de Monchenault , P. Jarry, B. Lenzi , E. Locci, J. Malcles, J. Rander, A. Rosowsky , M.Ö. Sahin , A. Savoy-Navarro¹⁶, M. Titov , G.B. Yu 

Laboratoire Leprince-Ringuet, CNRS/IN2P3, Ecole Polytechnique, Institut Polytechnique de Paris, Palaiseau, France

S. Ahuja , F. Beaudette , M. Bonanomi , A. Buchot Perraguin, P. Busson, A. Cappati, C. Charlot, O. Davignon, B. Diab, G. Falmagne , S. Ghosh, R. Granier de Cassagnac , A. Hakimi, I. Kucher , M. Nguyen , C. Ochando , P. Paganini , J. Rembser, R. Salerno , J.B. Sauvan , Y. Sirois , A. Zabi, A. Zghiche 

Université de Strasbourg, CNRS, IPHC UMR 7178, Strasbourg, France

J.-L. Agram¹⁷ , J. Andrea, D. Apparu, D. Bloch , G. Bourgatte, J.-M. Brom, E.C. Chabert, C. Collard , D. Darej, J.-C. Fontaine¹⁷, U. Goerlach, C. Grimault, A.-C. Le Bihan, E. Nibigira , P. Van Hove 

Institut de Physique des 2 Infinis de Lyon (IP2I), Villeurbanne, France

E. Asilar , S. Beauceron , C. Bernet , G. Boudoul, C. Camen, A. Carle, N. Chanon , D. Contardo, P. Depasse , H. El Mamouni, J. Fay, S. Gascon , M. Gouzevitch , B. Ille, I.B. Laktineh, H. Lattaud , A. Lesauvage , M. Lethuillier , L. Mirabito, S. Perries, K. Shchablo, V. Sordini , L. Torterotot , G. Touquet, M. Vander Donckt, S. Viret

Georgian Technical University, Tbilisi, Georgia

D. Lomidze , I. Lomidze, Z. Tsamalaidze¹²

RWTH Aachen University, I. Physikalisches Institut, Aachen, Germany

L. Feld , K. Klein, M. Lipinski, D. Meuser, A. Pauls, M.P. Rauch, N. Röwert, J. Schulz, M. Teroerde 

RWTH Aachen University, III. Physikalisches Institut A, Aachen, Germany

A. Dodonova, D. Eliseev, M. Erdmann , P. Fackeldey , B. Fischer, S. Ghosh , T. Hebbeker , K. Hoepfner, F. Ivone, H. Keller, L. Mastrolorenzo, M. Merschmeyer 

A. Meyer , G. Mocellin, S. Mondal, S. Mukherjee , D. Noll , A. Novak, T. Pook , A. Pozdnyakov , Y. Rath, H. Reithler, J. Roemer, A. Schmidt , S.C. Schuler, A. Sharma , L. Vigilante, S. Wiedenbeck, S. Zaleski

RWTH Aachen University, III. Physikalisches Institut B, Aachen, Germany

C. Dziwok, G. Flügge, W. Haj Ahmad¹⁸ , O. Hlushchenko, T. Kress, A. Nowack , C. Pistone, O. Pooth, D. Roy , H. Sert , A. Stahl¹⁹ , T. Ziemons 

Deutsches Elektronen-Synchrotron, Hamburg, Germany

H. Aarup Petersen, M. Aldaya Martin, P. Asmuss, I. Babounikau , S. Baxter, O. Behnke, A. Bermúdez Martínez, S. Bhattacharya, A.A. Bin Anuar , K. Borras²⁰, V. Botta, D. Brunner, A. Campbell , A. Cardini , C. Cheng, F. Colombina, S. Consuegra Rodríguez , G. Correia Silva, V. Danilov, L. Didukh, G. Eckerlin, D. Eckstein, L.I. Estevez Banos , O. Filatov , E. Gallo²¹, A. Geiser, A. Giraldi, A. Grohsjean , M. Guthoff, A. Jafari²² , N.Z. Jomhari , H. Jung , A. Kasem²⁰ , M. Kasemann , H. Kaveh , C. Kleinwort , D. Krücker , W. Lange, J. Lidrych , K. Lipka, W. Lohmann²³, R. Mankel, I.-A. Melzer-Pellmann , J. Metwally, A.B. Meyer , M. Meyer , J. Mnich , A. Mussgiller, Y. Otarid, D. Pérez Adán , D. Pitzl, A. Raspereza, B. Ribeiro Lopes, J. Rübenach, A. Saggio , A. Saibel , M. Savitskyi , M. Scham, V. Scheurer, C. Schwanenberger²¹ , A. Singh, R.E. Sosa Ricardo , D. Stafford, N. Tonon , O. Turkot , M. Van De Klundert , R. Walsh , D. Walter, Y. Wen , K. Wichmann, L. Wiens, C. Wissing, S. Wuchterl 

University of Hamburg, Hamburg, Germany

R. Aggleton, S. Albrecht , S. Bein , L. Benato , A. Benecke, P. Connor , K. De Leo , M. Eich, F. Feindt, A. Fröhlich, C. Garbers , E. Garutti , P. Gunnellini, J. Haller , A. Hinzmann , G. Kasieczka, R. Klanner , R. Kogler , T. Kramer, V. Kutzner, J. Lange , T. Lange , A. Lobanov , A. Malara , A. Nigamova, K.J. Pena Rodriguez, O. Rieger, P. Schleper, M. Schröder , J. Schwandt , D. Schwarz, J. Sonneveld , H. Stadie, G. Steinbrück, A. Tews, B. Vormwald , I. Zoi 

Karlsruher Institut fuer Technologie, Karlsruhe, Germany

J. Bechtel , T. Berger, E. Butz , R. Caspart , T. Chwalek, W. De Boer[†], A. Dierlamm, A. Droll, K. El Morabit, N. Faltermann , M. Giffels, J.o. Gosewisch, A. Gottmann, F. Hartmann¹⁹ , C. Heidecker, U. Husemann , I. Katkov²⁴, P. Keicher, R. Koppenhöfer, S. Maier, M. Metzler, S. Mitra , Th. Müller, M. Neukum, A. Nürnberg, G. Quast , K. Rabbertz , J. Rauser, D. Savoiu , M. Schnepf, D. Seith, I. Shvetsov, H.J. Simonis, R. Ulrich , J. Van Der Linden, R.F. Von Cube, M. Wassmer, M. Weber , S. Wieland, R. Wolf , S. Wozniewski, S. Wunsch

Institute of Nuclear and Particle Physics (INPP), NCSR Demokritos, Aghia Paraskevi, Greece

G. Anagnostou, G. Daskalakis, T. Geralis , A. Kyriakis, D. Loukas, A. Stakia 

National and Kapodistrian University of Athens, Athens, Greece

M. Diamantopoulou, D. Karasavvas, G. Karathanasis, P. Kontaxakis , C.K. Koraka, A. Manousakis-Katsikakis, A. Panagiotou, I. Papavergou, N. Saoulidou , K. Theofilatos , E. Tziaferi , K. Vellidis, E. Vourliotis

National Technical University of Athens, Athens, Greece

G. Bakas, K. Kousouris , I. Papakrivopoulos, G. Tsipolitis, A. Zacharopoulou

University of Ioánnina, Ioánnina, Greece

I. Evangelou , C. Foudas, P. Gianneios, P. Katsoulis, P. Kokkas, N. Manthos, I. Papadopoulos , J. Strologas 

MTA-ELTE Lendület CMS Particle and Nuclear Physics Group, Eötvös Loránd University, Budapest, Hungary

M. Csanad , K. Farkas, M.M.A. Gadallah²⁵ , S. Lökösz , P. Major, K. Mandal , A. Mehta , G. Pasztor , A.J. Rádl, O. Surányi, G.I. Veres 

Wigner Research Centre for Physics, Budapest, Hungary

M. Bartók²⁷ , G. Bencze, C. Hajdu , D. Horvath²⁸ , F. Sikler , V. Veszpremi , G. Vesztergombi[†]

Institute of Nuclear Research ATOMKI, Debrecen, Hungary

S. Czellar, J. Karancsi²⁷ , J. Molnar, Z. Szillasi, D. Teyssier

Institute of Physics, University of Debrecen, Debrecen, Hungary

P. Raics, Z.L. Trocsanyi²⁹ , B. Ujvari

Karoly Robert Campus, MATE Institute of Technology, Gyongyos, Hungary

T. Csorgo³⁰ , F. Nemes³⁰, T. Novak

Indian Institute of Science (IISc), Bangalore, India

J.R. Komaragiri , D. Kumar, L. Panwar , P.C. Tiwari 

National Institute of Science Education and Research, HBNI, Bhubaneswar, India

S. Bahinipati³¹ , C. Kar , P. Mal, T. Mishra , V.K. Muraleedharan Nair Bindhu³², A. Nayak³² , P. Saha, N. Sur , S.K. Swain, D. Vats³²

Punjab University, Chandigarh, India

S. Bansal , S.B. Beri, V. Bhatnagar , G. Chaudhary , S. Chauhan , N. Dhingra³³ , R. Gupta, A. Kaur, M. Kaur , S. Kaur, P. Kumari , M. Meena, K. Sandeep , J.B. Singh , A.K. Virdi 

University of Delhi, Delhi, India

A. Ahmed, A. Bhardwaj , B.C. Choudhary , M. Gola, S. Keshri , A. Kumar , M. Naimuddin , P. Priyanka , K. Ranjan, A. Shah 

Saha Institute of Nuclear Physics, HBNI, Kolkata, India

M. Bharti³⁴, R. Bhattacharya, S. Bhattacharya , D. Bhowmik, S. Dutta, S. Dutta, B. Gomber³⁵ , M. Maity³⁶, P. Palit , P.K. Rout , G. Saha, B. Sahu , S. Sarkar, M. Sharan, B. Singh³⁴, S. Thakur³⁴

Indian Institute of Technology Madras, Madras, India

P.K. Behera , S.C. Behera, P. Kalbhor , A. Muhammad, R. Pradhan, P.R. Pujahari, A. Sharma , A.K. Sikdar

Bhabha Atomic Research Centre, Mumbai, India

D. Dutta , V. Jha, V. Kumar , D.K. Mishra, K. Naskar³⁷, P.K. Netrakanti, L.M. Pant, P. Shukla 

Tata Institute of Fundamental Research-A, Mumbai, India

T. Aziz, S. Dugad, M. Kumar, U. Sarkar 

Tata Institute of Fundamental Research-B, Mumbai, India

S. Banerjee , R. Chudasama, M. Guchait, S. Karmakar, S. Kumar, G. Majumder, K. Mazumdar, S. Mukherjee 

Indian Institute of Science Education and Research (IISER), Pune, India

K. Alpana, S. Dube , B. Kansal, A. Laha, S. Pandey , A. Rane , A. Rastogi , S. Sharma 

Isfahan University of Technology, Isfahan, IranH. Bakhshiansohi³⁸ , M. Zeinali³⁹**Institute for Research in Fundamental Sciences (IPM), Tehran, Iran**S. Chenarani⁴⁰, S.M. Etesami , M. Khakzad , M. Mohammadi Najafabadi **University College Dublin, Dublin, Ireland**M. Grunewald **INFN Sezione di Bari ^a, Bari, Italy, Università di Bari ^b, Bari, Italy, Politecnico di Bari ^c, Bari, Italy**

M. Abbrescia^{a,b} , R. Aly^{a,b,41} , C. Aruta^{a,b}, A. Colaleo^a , D. Creanza^{a,c} , N. De Filippis^{a,c} , M. De Palma^{a,b} , A. Di Florio^{a,b}, A. Di Pilato^{a,b} , W. Elmetenawee^{a,b} , L. Fiore^a , A. Gelmi^{a,b} , M. Gul^a , G. Iaselli^{a,c} , M. Ince^{a,b} , S. Lezki^{a,b} , G. Maggi^{a,c} , M. Maggi^a , I. Margjeka^{a,b}, V. Mastrapasqua^{a,b} , J.A. Merlin^a, S. My^{a,b} , S. Nuzzo^{a,b} , A. Pellecchia^{a,b}, A. Pompili^{a,b} , G. Pugliese^{a,c} , A. Ranieri^a , G. Selvaggi^{a,b} , L. Silvestris^a , F.M. Simone^{a,b} , R. Venditti^a , P. Verwilligen^a 

INFN Sezione di Bologna ^a, Bologna, Italy, Università di Bologna ^b, Bologna, Italy

G. Abbiendi^a , C. Battilana^{a,b} , D. Bonacorsi^{a,b} , L. Borgonovi^a, L. Brigliadori^a, R. Campanini^{a,b} , P. Capiluppi^{a,b} , A. Castro^{a,b} , F.R. Cavallo^a , M. Cuffiani^{a,b} , G.M. Dallavalle^a , T. Diotalevi^{a,b} , F. Fabbri^a , A. Fanfani^{a,b} , P. Giacomelli^a , L. Giommi^{a,b} , C. Grandi^a , L. Guiducci^{a,b}, S. Lo Meo^{a,42}, L. Lunerti^{a,b}, S. Marcellini^a , G. Masetti^a , F.L. Navarreria^{a,b} , A. Perrotta^a , F. Primavera^{a,b} , A.M. Rossi^{a,b} , T. Rovelli^{a,b} , G.P. Siroli^{a,b} 

INFN Sezione di Catania ^a, Catania, Italy, Università di Catania ^b, Catania, Italy

S. Albergo^{a,b,43} , S. Costa^{a,b,43} , A. Di Mattia^a , R. Potenza^{a,b}, A. Tricomi^{a,b,43} , C. Tuve^{a,b} 

INFN Sezione di Firenze ^a, Firenze, Italy, Università di Firenze ^b, Firenze, Italy

G. Barbagli^a , A. Cassese^a , R. Ceccarelli^{a,b}, V. Ciulli^{a,b} , C. Civinini^a , R. D'Alessandro^{a,b} , E. Focardia^{a,b} , G. Latino^{a,b} , P. Lenzi^{a,b} , M. Lizzo^{a,b}, M. Meschini^a , S. Paoletti^a , R. Seidita^{a,b}, G. Sguazzoni^a , L. Viliani^a 

INFN Laboratori Nazionali di Frascati, Frascati, ItalyL. Benussi , S. Bianco , D. Piccolo **INFN Sezione di Genova ^a, Genova, Italy, Università di Genova ^b, Genova, Italy**M. Bozzo^{a,b} , F. Ferro^a , R. Mulargia^{a,b}, E. Robutti^a , S. Tosi^{a,b} **INFN Sezione di Milano-Bicocca ^a, Milano, Italy, Università di Milano-Bicocca ^b, Milano, Italy**

A. Benaglia^a , F. Brivio^{a,b}, F. Cetorelli^{a,b}, V. Ciriolo^{a,b,19}, F. De Guio^{a,b} , M.E. Dinardo^{a,b} , P. Dini^a , S. Gennai^a , A. Ghezzi^{a,b} , P. Govoni^{a,b} , L. Guzzi^{a,b} , M. Malberti^a, S. Malvezzi^a , A. Massironi^a , D. Menasce^a , L. Moroni^a , M. Paganoni^{a,b} , D. Pedrini^a , S. Ragazzi^{a,b} , N. Redaelli^a , T. Tabarelli de Fatis^{a,b} , D. Valsecchi^{a,b,19}, D. Zuolo^{a,b} 

INFN Sezione di Napoli ^a, Napoli, Italy, Università di Napoli 'Federico II' ^b, Napoli, Italy, Università della Basilicata ^c, Potenza, Italy, Università G. Marconi ^d, Roma, Italy

S. Buontempo^a , F. Carnevali^{a,b}, N. Cavallo^{a,c} , A. De Iorio^{a,b} , F. Fabozzi^{a,c} , A.O.M. Iorio^{a,b} , L. Lista^{a,b} , S. Meola^{a,d,19} , P. Paolucci^{a,19} , B. Rossi^a , C. Sciacca^{a,b} 

INFN Sezione di Padova ^a, Padova, Italy, Università di Padova ^b, Padova, Italy, Università

di Trento ^c, Trento, Italy

P. Azzi^a , N. Bacchetta^a , D. Bisello^{a,b} , P. Bortignon^a , A. Bragagnolo^{a,b} , R. Carlin^{a,b} , P. Checchia^a , T. Dorigo^a , U. Dosselli^a , F. Gasparini^{a,b} , U. Gasparini^{a,b} , S.Y. Hoh^{a,b} , L. Layer^{a,44}, M. Margoni^{a,b} , A.T. Meneguzzo^{a,b} , J. Pazzini^{a,b} , M. Presilla^{a,b} , P. Ronchese^{a,b} , R. Rossin^{a,b}, F. Simonetto^{a,b} , G. Strong^a , M. Tosi^{a,b} , H. YARAR^{a,b}, M. Zanetti^{a,b} , P. Zotto^{a,b} , A. Zucchetta^{a,b} , G. Zumerle^{a,b}

INFN Sezione di Pavia ^a, Pavia, Italy, Università di Pavia ^b, Pavia, Italy

C. Aime^{a,b}, A. Braghieri^a , S. Calzaferri^{a,b}, D. Fiorina^{a,b} , P. Montagna^{a,b}, S.P. Ratti^{a,b}, V. Re^a , C. Riccardi^{a,b} , P. Salvini^a , I. Vai^a , P. Vitulò^{a,b} 

INFN Sezione di Perugia ^a, Perugia, Italy, Università di Perugia ^b, Perugia, Italy

P. Asenov^{a,45} , G.M. Bilei^a , D. Ciangottini^{a,b} , L. Fanò^{a,b} , P. Lariccia^{a,b}, M. Magherini^b, G. Mantovani^{a,b}, V. Mariani^{a,b}, M. Menichelli^a , F. Moscatelli^{a,45} , A. Piccinelli^{a,b} , A. Rossi^{a,b} , A. Santocchia^{a,b} , D. Spiga^a , T. Tedeschi^{a,b}

INFN Sezione di Pisa ^a, Pisa, Italy, Università di Pisa ^b, Pisa, Italy, Scuola Normale Superiore di Pisa ^c, Pisa, Italy, Università di Siena ^d, Siena, Italy

P. Azzurri^a , G. Bagliesi^a , V. Bertacchi^{a,c} , L. Bianchini^a , T. Boccali^a , E. Bossini^{a,b} , R. Castaldi^a , M.A. Ciocci^{a,b} , V. D'Amante^{a,d} , R. Dell'Orso^a , M.R. Di Domenico^{a,d} , S. Donato^a , A. Giassi^a , F. Ligabue^{a,c} , E. Manca^{a,c} , G. Mandorli^{a,c} , A. Messineo^{a,b} , F. Palla^a , S. Parolia^{a,b}, G. Ramirez-Sanchez^{a,c}, A. Rizzi^{a,b} , G. Rolandi^{a,c} , S. Roy Chowdhury^{a,c}, A. Scribano^a, N. Shafiei^{a,b} , P. Spagnolo^a , R. Tenchini^a , G. Tonelli^{a,b} , N. Turini^{a,d} , A. Venturi^a , P.G. Verdini^a

INFN Sezione di Roma ^a, Rome, Italy, Sapienza Università di Roma ^b, Rome, Italy

M. Campana^{a,b}, F. Cavallari^a , D. Del Re^{a,b} , E. Di Marco^a , M. Diemoz^a , E. Longo^{a,b} , P. Meridiani^a , G. Organtini^{a,b} , F. Pandolfi^a, R. Paramatti^{a,b} , C. Quaranta^{a,b}, S. Rahatlou^{a,b} , C. Rovelli^a , F. Santanastasio^{a,b} , L. Soffi^a , R. Tramontano^{a,b}

INFN Sezione di Torino ^a, Torino, Italy, Università di Torino ^b, Torino, Italy, Università del Piemonte Orientale ^c, Novara, Italy

N. Amapane^{a,b} , R. Arcidiacono^{a,c} , S. Argiro^{a,b} , M. Arneodo^{a,c} , N. Bartosik^a , R. Bellan^{a,b} , A. Bellora^{a,b} , J. Berenguer Antequera^{a,b} , C. Biino^a , N. Cartiglia^a , S. Cometti^a , M. Costa^{a,b} , R. Covarelli^{a,b} , N. Demaria^a , B. Kiani^{a,b} , F. Legger^a , C. Mariotti^a , S. Maselli^a , E. Migliore^{a,b} , E. Monteil^{a,b} , M. Monteno^a , M.M. Obertino^{a,b} , G. Ortona^a , L. Pacher^{a,b} , N. Pastrone^a , M. Pelliccioni^a , G.L. Pinna Angioni^{a,b}, M. Ruspa^{a,c} , K. Shchelina^{a,b} , F. Siviero^{a,b} , V. Sola^a , A. Solano^{a,b} , D. Soldi^{a,b} , A. Staiano^a , M. Tornago^{a,b} , D. Trocino^{a,b} , A. Vagnerini

INFN Sezione di Trieste ^a, Trieste, Italy, Università di Trieste ^b, Trieste, Italy

S. Belforte^a , V. Candelise^{a,b} , M. Casarsa^a , F. Cossutti^a , A. Da Rold^{a,b} , G. Della Ricca^{a,b} , G. Sorrentino^{a,b}, F. Vazzoler^{a,b} 

Kyungpook National University, Daegu, Korea

S. Dogra , C. Huh , B. Kim, D.H. Kim , G.N. Kim , J. Kim, J. Lee, S.W. Lee , C.S. Moon , Y.D. Oh , S.I. Pak, B.C. Radburn-Smith, S. Sekmen , Y.C. Yang

Chonnam National University, Institute for Universe and Elementary Particles, Kwangju, Korea

H. Kim , D.H. Moon 

Hanyang University, Seoul, Korea

B. Francois , T.J. Kim , J. Park 

Korea University, Seoul, Korea

S. Cho, S. Choi , Y. Go, B. Hong , K. Lee, K.S. Lee , J. Lim, J. Park, S.K. Park, J. Yoo

Kyung Hee University, Department of Physics, Seoul, Republic of Korea, Seoul, Korea

J. Goh , A. Gurtu

Sejong University, Seoul, Korea

H.S. Kim , Y. Kim

Seoul National University, Seoul, Korea

J. Almond, J.H. Bhyun, J. Choi, S. Jeon, J. Kim, J.S. Kim, S. Ko, H. Kwon, H. Lee , S. Lee, B.H. Oh, M. Oh , S.B. Oh, H. Seo , U.K. Yang, I. Yoon 

University of Seoul, Seoul, Korea

W. Jang, D. Jeon, D.Y. Kang, Y. Kang, J.H. Kim, S. Kim, B. Ko, J.S.H. Lee , Y. Lee, I.C. Park, Y. Roh, M.S. Ryu, D. Song, I.J. Watson , S. Yang

Yonsei University, Department of Physics, Seoul, Korea

S. Ha, H.D. Yoo

Sungkyunkwan University, Suwon, Korea

M. Choi, Y. Jeong, H. Lee, Y. Lee, I. Yu 

College of Engineering and Technology, American University of the Middle East (AUM), Egaila, Kuwait, Dasman, Kuwait

T. Beyrouthy, Y. Maghrbi

Riga Technical University, Riga, Latvia

T. Torims, V. Veckalns⁴⁶ 

Vilnius University, Vilnius, Lithuania

M. Ambrozas, A. Carvalho Antunes De Oliveira , A. Juodagalvis , A. Rinkevicius , G. Tamulaitis 

National Centre for Particle Physics, Universiti Malaya, Kuala Lumpur, Malaysia

N. Bin Norjoharuddeen , W.A.T. Wan Abdullah, M.N. Yusli, Z. Zolkapli

Universidad de Sonora (UNISON), Hermosillo, Mexico

J.F. Benitez , A. Castaneda Hernandez , M. León Coello, J.A. Murillo Quijada , A. Sehrawat, L. Valencia Palomo 

Centro de Investigacion y de Estudios Avanzados del IPN, Mexico City, Mexico

G. Ayala, H. Castilla-Valdez, E. De La Cruz-Burelo , I. Heredia-De La Cruz⁴⁷ , R. Lopez-Fernandez, C.A. Mondragon Herrera, D.A. Perez Navarro, A. Sánchez Hernández 

Universidad Iberoamericana, Mexico City, Mexico

S. Carrillo Moreno, C. Oropeza Barrera , M. Ramírez García , F. Vazquez Valencia

Benemerita Universidad Autonoma de Puebla, Puebla, Mexico

I. Pedraza, H.A. Salazar Ibarguen, C. Uribe Estrada

University of Montenegro, Podgorica, Montenegro

J. Mijuskovic⁴⁸, N. Raicevic

University of Auckland, Auckland, New Zealand

D. Kofcheck 

University of Canterbury, Christchurch, New Zealand
 S. Bheesette, P.H. Butler 

National Centre for Physics, Quaid-I-Azam University, Islamabad, Pakistan
 A. Ahmad, M.I. Asghar, A. Awais, M.I.M. Awan, H.R. Hoorani, W.A. Khan, M.A. Shah, M. Shoaib , M. Waqas 

AGH University of Science and Technology Faculty of Computer Science, Electronics and Telecommunications, Krakow, Poland
 V. Avati, L. Grzanka, M. Malawski

National Centre for Nuclear Research, Swierk, Poland
 H. Bialkowska, M. Bluj , B. Boimska , M. Górski, M. Kazana, M. Szleper , P. Zalewski

Institute of Experimental Physics, Faculty of Physics, University of Warsaw, Warsaw, Poland
 K. Bunkowski, K. Doroba, A. Kalinowski , M. Konecki , J. Krolikowski , M. Walczak 

Laboratório de Instrumentação e Física Experimental de Partículas, Lisboa, Portugal
 M. Araujo, P. Bargassa , D. Bastos, A. Boletti , P. Faccioli , M. Gallinaro , J. Hollar , N. Leonardo , T. Niknejad, M. Pisano, J. Seixas , O. Toldaiev , J. Varela 

Joint Institute for Nuclear Research, Dubna, Russia
 S. Afanasiev, D. Budkouski, I. Golutvin, I. Gorbunov , V. Karjavine, V. Korenkov , A. Lanev, A. Malakhov, V. Matveev^{49,50}, V. Palichik, V. Perelygin, M. Savina, D. Seitova, V. Shalaev, S. Shmatov, S. Shulha, V. Smirnov, O. Teryaev, N. Voityshin, B.S. Yuldashev⁵¹, A. Zarubin, I. Zhizhin

Petersburg Nuclear Physics Institute, Gatchina (St. Petersburg), Russia
 G. Gavrilov , V. Golovtcov, Y. Ivanov, V. Kim⁵² , E. Kuznetsova⁵³, V. Murzin, V. Oreshkin, I. Smirnov, D. Sosnov , V. Sulimov, L. Uvarov, S. Volkov, A. Vorobyev

Institute for Nuclear Research, Moscow, Russia
 Yu. Andreev , A. Dermenev, S. Glinenko , N. Golubev, A. Karneyeu , D. Kirpichnikov , M. Kirsanov, N. Krasnikov, A. Pashenkov, G. Pivovarov , D. Tlisov[†], A. Toropin

Institute for Theoretical and Experimental Physics named by A.I. Alikhanov of NRC ‘Kurchatov Institute’, Moscow, Russia
 V. Epshteyn, V. Gavrilov, N. Lychkovskaya, A. Nikitenko⁵⁴, V. Popov, A. Spiridonov, A. Stepenov, M. Toms, E. Vlasov , A. Zhokin

Moscow Institute of Physics and Technology, Moscow, Russia
 T. Aushev

National Research Nuclear University ‘Moscow Engineering Physics Institute’ (MEPhI), Moscow, Russia
 O. Bychkova, M. Chadeeva⁵⁵ , P. Parygin, E. Popova, E. Zhemchugov⁵⁶ 

P.N. Lebedev Physical Institute, Moscow, Russia
 V. Andreev, M. Azarkin, I. Dremin , M. Kirakosyan, A. Terkulov

Skobeltsyn Institute of Nuclear Physics, Lomonosov Moscow State University, Moscow, Russia
 A. Belyaev, E. Boos , V. Bunichev, M. Dubinin⁵⁷ , L. Dudko , A. Ershov, V. Klyukhin , O. Kodolova , I. Lokhtin , S. Obraztsov, M. Perfilov, V. Savrin, A. Snigirev 

Novosibirsk State University (NSU), Novosibirsk, Russia

V. Blinov⁵⁸, T. Dimova⁵⁸, L. Kardapoltsev⁵⁸, A. Kozyrev⁵⁸, I. Ovtin⁵⁸, Y. Skovpen⁵⁸ 

Institute for High Energy Physics of National Research Centre 'Kurchatov Institute', Protvino, Russia

I. Azhgirey , I. Bayshev, D. Elumakhov, V. Kachanov, D. Konstantinov , P. Mandrik , V. Petrov, R. Ryutin, S. Slabospitskii , A. Sobol, S. Troshin , N. Tyurin, A. Uzunian, A. Volkov

National Research Tomsk Polytechnic University, Tomsk, Russia

A. Babaev, V. Okhotnikov

Tomsk State University, Tomsk, Russia

V. Borshch, V. Ivanchenko , E. Tcherniaev 

University of Belgrade: Faculty of Physics and VINCA Institute of Nuclear Sciences, Belgrade, Serbia

P. Adzic⁵⁹ , M. Dordevic , P. Milenovic , J. Milosevic 

Centro de Investigaciones Energéticas Medioambientales y Tecnológicas (CIEMAT), Madrid, Spain

M. Aguilar-Benitez, J. Alcaraz Maestre , A. Álvarez Fernández, I. Bachiller, M. Barrio Luna, Cristina F. Bedoya , C.A. Carrillo Montoya , M. Cepeda , M. Cerrada, N. Colino , B. De La Cruz, A. Delgado Peris , J.P. Fernández Ramos , J. Flix , M.C. Fouz , O. Gonzalez Lopez , S. Goy Lopez , J.M. Hernandez , M.I. Josa , J. León Holgado , D. Moran, Á. Navarro Tobar , A. Pérez-Calero Yzquierdo , J. Puerta Pelayo , I. Redondo , L. Romero, S. Sánchez Navas, L. Urda Gómez , C. Willmott

Universidad Autónoma de Madrid, Madrid, Spain

J.F. de Trocóniz, R. Reyes-Almanza 

Universidad de Oviedo, Instituto Universitario de Ciencias y Tecnologías Espaciales de Asturias (ICTEA), Oviedo, Spain

B. Alvarez Gonzalez , J. Cuevas , C. Erice , J. Fernandez Menendez , S. Folgueras , I. Gonzalez Caballero , J.R. González Fernández, E. Palencia Cortezon , C. Ramón Álvarez, J. Ripoll Sau, V. Rodríguez Bouza , A. Trapote, N. Trevisani 

Instituto de Física de Cantabria (IFCA), CSIC-Universidad de Cantabria, Santander, Spain

J.A. Brochero Cifuentes , I.J. Cabrillo, A. Calderon , J. Duarte Campderros , M. Fernández , C. Fernandez Madrazo , P.J. Fernández Manteca , A. García Alonso, G. Gomez, C. Martinez Rivero, P. Martinez Ruiz del Arbol , F. Matorras , P. Matorras Cuevas , J. Piedra Gomez , C. Prieels, T. Rodrigo , A. Ruiz-Jimeno , L. Scodellaro , I. Vila, J.M. Vizan Garcia 

University of Colombo, Colombo, Sri Lanka

M.K. Jayananda, B. Kailasapathy⁶⁰, D.U.J. Sonnadara, D.D.C. Wickramarathna

University of Ruhuna, Department of Physics, Matara, Sri Lanka

W.G.D. Dharmaratna , K. Liyanage, N. Perera, N. Wickramage

CERN, European Organization for Nuclear Research, Geneva, Switzerland

T.K. Arrestad , D. Abbaneo, J. Alimena , E. Auffray, G. Auzinger, J. Baechler, P. Baillon[†], D. Barney , J. Bendavid, M. Bianco , A. Bocci , T. Camporesi, M. Capeans Garrido , G. Cerminara, S.S. Chhibra , M. Cipriani , L. Cristella , D. d'Enterria , A. Dabrowski , N. Daci , A. David , A. De Roeck , M.M. Defranchis , M. Deile , M. Dobson, M. Dünser , N. Dupont, A. Elliott-Peisert, N. Emriskova, F. Fallavollita⁶¹, D. Fasanella , S. Fiorendi , A. Florent , G. Franzoni , W. Funk, S. Giani, D. Gigi, K. Gill, F. Glege,

L. Gouskos , M. Haranko , J. Hegeman , Y. Iiyama , V. Innocente , T. James, P. Janot , J. Kaspar , J. Kieseler , M. Komm , N. Kratochwil, C. Lange , S. Laurila, P. Lecoq , K. Long , C. Lourenço , L. Malgeri , S. Mallios, M. Mannelli, A.C. Marini , F. Meijers, S. Mersi , E. Meschi , F. Moortgat , M. Mulders , S. Orfanelli, L. Orsini, F. Pantaleo , L. Pape, E. Perez, M. Peruzzi , A. Petrilli, G. Petrucciani , A. Pfeiffer , M. Pierini , D. Piparo, M. Pitt , H. Qu , T. Quast, D. Rabady , A. Racz, G. Reales Gutiérrez, M. Rieger , M. Rovere, H. Sakulin, J. Salfeld-Nebgen , S. Scarfi, C. Schäfer, C. Schwick, M. Selvaggi , A. Sharma, P. Silva , W. Snoeys , P. Sphicas⁶² , S. Summers , V.R. Tavolaro , D. Treille, A. Tsirou, G.P. Van Onsem , M. Verzetti , J. Wanczyk⁶³, K.A. Wozniak, W.D. Zeuner

Paul Scherrer Institut, Villigen, Switzerland

L. Caminada⁶⁴ , A. Ebrahimi , W. Erdmann, R. Horisberger, Q. Ingram, H.C. Kaestli, D. Kotlinski, U. Langenegger, M. Missiroli , T. Rohe

ETH Zurich - Institute for Particle Physics and Astrophysics (IPA), Zurich, Switzerland

K. Androsov⁶³ , M. Backhaus , P. Berger, A. Calandri , N. Chernyavskaya , A. De Cosa, G. Dissertori , M. Dittmar, M. Donegà, C. Dorfer , F. Eble, K. Gedia, F. Glessgen, T.A. Gómez Espinosa , C. Grab , D. Hits, W. Lustermann, A.-M. Lyon, R.A. Manzoni , C. Martin Perez, M.T. Meinhard, F. Nessi-Tedaldi, J. Niedziela , F. Pauss, V. Perovic, S. Pigazzini , M.G. Ratti , M. Reichmann, C. Reissel, T. Reitenspiess, B. Ristic , D. Ruini, D.A. Sanz Becerra , M. Schönenberger , V. Stampf, J. Steggemann⁶³ , R. Wallny , D.H. Zhu

Universität Zürich, Zurich, Switzerland

C. Amsler⁶⁵ , P. Bärtschi, C. Botta , D. Brzhechko, M.F. Canelli , K. Cormier, A. De Wit , R. Del Burgo, J.K. Heikkilä , M. Huwiler, A. Jofrehei , B. Kilminster , S. Leontsinis , A. Macchiolo , P. Meiring, V.M. Mikuni , U. Molinatti, I. Neutelings, A. Reimers, P. Robmann, S. Sanchez Cruz , K. Schweiger , Y. Takahashi

National Central University, Chung-Li, Taiwan

C. Adloff⁶⁶, C.M. Kuo, W. Lin, A. Roy , T. Sarkar³⁶ , S.S. Yu

National Taiwan University (NTU), Taipei, Taiwan

L. Ceard, Y. Chao, K.F. Chen , P.H. Chen , W.-S. Hou , Y.y. Li, R.-S. Lu, E. Paganis , A. Psallidas, A. Steen, H.y. Wu, E. Yazgan , P.r. Yu

Chulalongkorn University, Faculty of Science, Department of Physics, Bangkok, Thailand

B. Asavapibhop , C. Asawatangtrakuldee , N. Srimanobhas 

Çukurova University, Physics Department, Science and Art Faculty, Adana, Turkey

F. Boran , S. Damarseckin⁶⁷, Z.S. Demiroglu , F. Dolek , I. Dumanoglu⁶⁸ , E. Eskut, Y. Guler , E. Gurpinar Guler⁶⁹ , I. Hos⁷⁰, C. Isik, O. Kara, A. Kayis Topaksu, U. Kiminsu , G. Onengut, K. Ozdemir⁷¹, A. Polatoz, A.E. Simsek , B. Tali⁷², U.G. Tok , S. Turkcapar, I.S. Zorbakir , C. Zorbilmez

Middle East Technical University, Physics Department, Ankara, Turkey

B. Isildak⁷³, G. Karapinar⁷⁴, K. Ocalan⁷⁵ , M. Yalvac⁷⁶ 

Bogazici University, Istanbul, Turkey

B. Akgun, I.O. Atakisi , E. Gülmез , M. Kaya⁷⁷ , O. Kaya⁷⁸, Ö. Özçelik, S. Tekten⁷⁹, E.A. Yetkin⁸⁰ 

Istanbul Technical University, Istanbul, Turkey

A. Cakir , K. Cankocak⁶⁸ , Y. Komurcu, S. Sen⁸¹ 

Istanbul University, Istanbul, Turkey

S. Cerci⁷², B. Kaynak, S. Ozkorucuklu, D. Sunar Cerci⁷² 

Institute for Scintillation Materials of National Academy of Science of Ukraine, Kharkov, Ukraine

B. Grynyov

National Scientific Center, Kharkov Institute of Physics and Technology, Kharkov, Ukraine

L. Levchuk 

University of Bristol, Bristol, United Kingdom

D. Anthony, E. Bhal , S. Bologna, J.J. Brooke , A. Bundock , E. Clement , D. Cussans , H. Flacher , J. Goldstein , G.P. Heath, H.F. Heath , M.-L. Holmberg⁸², L. Kreczko , B. Krikler , S. Paramesvaran, S. Seif El Nasr-Storey, V.J. Smith, N. Stylianou⁸³ , K. Walkingshaw Pass, R. White

Rutherford Appleton Laboratory, Didcot, United Kingdom

K.W. Bell, A. Belyaev⁸⁴ , C. Brew , R.M. Brown, D.J.A. Cockerill, C. Cooke, K.V. Ellis, K. Harder, S. Harper, J. Linacre , K. Manolopoulos, D.M. Newbold , E. Olaiya, D. Petyt, T. Reis , T. Schuh, C.H. Shepherd-Themistocleous, I.R. Tomalin, T. Williams 

Imperial College, London, United Kingdom

R. Bainbridge , P. Bloch , S. Bonomally, J. Borg , S. Breeze, O. Buchmuller, V. Cepaitis , G.S. Chahal⁸⁵ , D. Colling, P. Dauncey , G. Davies , M. Della Negra , S. Fayer, G. Fedi , G. Hall , M.H. Hassanshahi, G. Iles, J. Langford, L. Lyons, A.-M. Magnan, S. Malik, A. Martelli , D.G. Monk, J. Nash⁸⁶ , M. Pesaresi, D.M. Raymond, A. Richards, A. Rose, E. Scott , C. Seez, A. Shtipliyski, A. Tapper , K. Uchida, T. Virdee¹⁹ , M. Vojinovic , N. Wardle , S.N. Webb , D. Winterbottom, A.G. Zecchinelli

Brunel University, Uxbridge, United Kingdom

K. Coldham, J.E. Cole , A. Khan, P. Kyberd , I.D. Reid , L. Teodorescu, S. Zahid 

Baylor University, Waco, Texas, USA

S. Abdullin , A. Brinkerhoff , B. Caraway , J. Dittmann , K. Hatakeyama , A.R. Kanuganti, B. McMaster , N. Pastika, M. Saunders , S. Sawant, C. Sutantawibul, J. Wilson 

Catholic University of America, Washington, DC, USA

R. Bartek , A. Dominguez , R. Uniyal , A.M. Vargas Hernandez

The University of Alabama, Tuscaloosa, Alabama, USA

A. Buccilli , S.I. Cooper , D. Di Croce , S.V. Gleyzer , C. Henderson , C.U. Perez , P. Rumerio⁸⁷ , C. West 

Boston University, Boston, Massachusetts, USA

A. Akpinar , A. Albert , D. Arcaro , C. Cosby , Z. Demiragli , E. Fontanesi, D. Gastler, J. Rohlf , K. Salyer , D. Sperka, D. Spitzbart , I. Suarez , A. Tsatsos, S. Yuan, D. Zou

Brown University, Providence, Rhode Island, USA

G. Benelli , B. Burkle , X. Coubez²⁰, D. Cutts , M. Hadley , U. Heintz , J.M. Hogan⁸⁸ , G. Landsberg , K.T. Lau , M. Lukasik, J. Luo , M. Narain, S. Sagir⁸⁹ , E. Usai , W.Y. Wong, X. Yan , D. Yu , W. Zhang

University of California, Davis, Davis, California, USA

J. Bonilla [ID](#), C. Brainerd [ID](#), R. Breedon, M. Calderon De La Barca Sanchez, M. Chertok [ID](#), J. Conway [ID](#), P.T. Cox, R. Erbacher, G. Haza, F. Jensen [ID](#), O. Kukral, R. Lander, M. Mulhearn [ID](#), D. Pellett, B. Regnery [ID](#), D. Taylor [ID](#), Y. Yao [ID](#), F. Zhang [ID](#)

University of California, Los Angeles, California, USA

M. Bachtis [ID](#), R. Cousins [ID](#), A. Datta [ID](#), D. Hamilton, J. Hauser [ID](#), M. Ignatenko, M.A. Iqbal, T. Lam, W.A. Nash, S. Regnard [ID](#), D. Saltzberg [ID](#), B. Stone, V. Valuev [ID](#)

University of California, Riverside, Riverside, California, USA

K. Burt, Y. Chen, R. Clare [ID](#), J.W. Gary [ID](#), M. Gordon, G. Hanson [ID](#), G. Karapostoli [ID](#), O.R. Long [ID](#), N. Manganelli, M. Olmedo Negrete, W. Si [ID](#), S. Wimpenny, Y. Zhang

University of California, San Diego, La Jolla, California, USA

J.G. Branson, P. Chang [ID](#), S. Cittolin, S. Cooperstein [ID](#), N. Deelen [ID](#), D. Diaz [ID](#), J. Duarte [ID](#), R. Gerosa [ID](#), L. Giannini [ID](#), D. Gilbert [ID](#), J. Guiang, R. Kansal [ID](#), V. Krutelyov [ID](#), R. Lee, J. Letts [ID](#), M. Masciovecchio [ID](#), S. May [ID](#), M. Pieri [ID](#), B.V. Sathia Narayanan [ID](#), V. Sharma [ID](#), M. Tadel, A. Vartak [ID](#), F. Würthwein [ID](#), Y. Xiang [ID](#), A. Yagil [ID](#)

University of California, Santa Barbara - Department of Physics, Santa Barbara, California, USA

N. Amin, C. Campagnari [ID](#), M. Citron [ID](#), A. Dorsett, V. Dutta [ID](#), J. Incandela [ID](#), M. Kilpatrick [ID](#), J. Kim [ID](#), B. Marsh, H. Mei, M. Oshiro, M. Quinnan [ID](#), J. Richman, U. Sarica [ID](#), J. Sheplock, D. Stuart, S. Wang [ID](#)

California Institute of Technology, Pasadena, California, USA

A. Bornheim [ID](#), O. Cerri, I. Dutta [ID](#), J.M. Lawhorn [ID](#), N. Lu [ID](#), J. Mao, H.B. Newman [ID](#), J. Ngadiuba [ID](#), T.Q. Nguyen [ID](#), M. Spiropulu [ID](#), J.R. Vlimant [ID](#), C. Wang [ID](#), S. Xie [ID](#), Z. Zhang [ID](#), R.Y. Zhu [ID](#)

Carnegie Mellon University, Pittsburgh, Pennsylvania, USA

J. Alison [ID](#), S. An [ID](#), M.B. Andrews, P. Bryant [ID](#), T. Ferguson [ID](#), A. Harilal, C. Liu, T. Mudholkar [ID](#), M. Paulini [ID](#), A. Sanchez

University of Colorado Boulder, Boulder, Colorado, USA

J.P. Cumalat [ID](#), W.T. Ford [ID](#), A. Hassani, E. MacDonald, R. Patel, A. Perloff [ID](#), C. Savard, K. Stenson [ID](#), K.A. Ulmer [ID](#), S.R. Wagner [ID](#)

Cornell University, Ithaca, New York, USA

J. Alexander [ID](#), S. Bright-Thonney [ID](#), Y. Cheng [ID](#), D.J. Cranshaw [ID](#), S. Hogan, J. Monroy [ID](#), J.R. Patterson [ID](#), D. Quach [ID](#), J. Reichert [ID](#), M. Reid [ID](#), A. Ryd, W. Sun [ID](#), J. Thom [ID](#), P. Wittich [ID](#), R. Zou [ID](#)

Fermi National Accelerator Laboratory, Batavia, Illinois, USA

M. Albrow [ID](#), M. Alyari [ID](#), G. Apollinari, A. Apresyan [ID](#), A. Apyan [ID](#), S. Banerjee, L.A.T. Bauerdtick [ID](#), D. Berry [ID](#), J. Berryhill [ID](#), P.C. Bhat, K. Burkett [ID](#), J.N. Butler, A. Canepa, G.B. Cerati [ID](#), H.W.K. Cheung [ID](#), F. Chlebana, M. Cremonesi, K.F. Di Petrillo [ID](#), V.D. Elvira [ID](#), Y. Feng, J. Freeman, Z. Gecse, L. Gray, D. Green, S. Grünendahl [ID](#), O. Gutsche [ID](#), R.M. Harris [ID](#), R. Heller, T.C. Herwig [ID](#), J. Hirschauer [ID](#), B. Jayatilaka [ID](#), S. Jindariani, M. Johnson, U. Joshi, T. Klijnsma [ID](#), B. Klima [ID](#), K.H.M. Kwok, S. Lammel [ID](#), D. Lincoln [ID](#), R. Lipton, T. Liu, C. Madrid, K. Maeshima, C. Mantilla [ID](#), D. Mason, P. McBride [ID](#), P. Merkel, S. Mrenna [ID](#), S. Nahm [ID](#), V. O'Dell, V. Papadimitriou, K. Pedro [ID](#), C. Pena⁵⁷ [ID](#), O. Prokofyev, F. Ravera [ID](#), A. Reinsvold Hall [ID](#), L. Ristori [ID](#), B. Schneider [ID](#), E. Sexton-Kennedy [ID](#), N. Smith [ID](#), A. Soha [ID](#), W.J. Spalding [ID](#), L. Spiegel, S. Stoynev [ID](#), J. Strait [ID](#), L. Taylor [ID](#), S. Tkaczyk, N.V. Tran [ID](#), L. Uplegger [ID](#), E.W. Vaandering [ID](#), H.A. Weber [ID](#)

University of Florida, Gainesville, Florida, USA

D. Acosta , P. Avery, D. Bourilkov , L. Cadamuro , V. Cherepanov, F. Errico , R.D. Field, D. Guerrero, B.M. Joshi , M. Kim, E. Koenig, J. Konigsberg , A. Korytov, K.H. Lo, K. Matchev , N. Menendez , G. Mitselmakher , A. Muthirakalayil Madhu, N. Rawal, D. Rosenzweig, S. Rosenzweig, K. Shi , J. Sturdy , J. Wang , E. Yigitbasi , X. Zuo

Florida State University, Tallahassee, Florida, USA

T. Adams , A. Askew , R. Habibullah , V. Hagopian, K.F. Johnson, R. Khurana, T. Kolberg , G. Martinez, H. Prosper , C. Schiber, O. Viazlo , R. Yohay , J. Zhang

Florida Institute of Technology, Melbourne, Florida, USA

M.M. Baarmand , S. Butalla, T. Elkafrawy¹⁵ , M. Hohlmann , R. Kumar Verma , D. Noonan , M. Rahmani, F. Yumiceva 

University of Illinois at Chicago (UIC), Chicago, Illinois, USA

M.R. Adams, H. Becerril Gonzalez , R. Cavanaugh , X. Chen , S. Dittmer, O. Evdokimov , C.E. Gerber , D.A. Hangal , D.J. Hofman , A.H. Merrit, C. Mills , G. Oh , T. Roy, S. Rudrabhatla, M.B. Tonjes , N. Varelas , J. Viinikainen , X. Wang, Z. Wu , Z. Ye 

The University of Iowa, Iowa City, Iowa, USA

M. Alhusseini , K. Dilsiz⁹⁰ , R.P. Gandrajula , O.K. Köseyan , J.-P. Merlo, A. Mestvirishvili⁹¹, J. Nachtman, H. Ogul⁹² , Y. Onel , A. Penzo, C. Snyder, E. Tiras⁹³ 

Johns Hopkins University, Baltimore, Maryland, USA

O. Amram , B. Blumenfeld , L. Corcodilos , J. Davis, M. Eminizer , A.V. Gritsan , S. Kyriacou, P. Maksimovic , J. Roskes , M. Swartz, T.Á. Vámi 

The University of Kansas, Lawrence, Kansas, USA

A. Abreu, J. Anguiano, C. Baldenegro Barrera , P. Baringer , A. Bean , A. Bylinkin , Z. Flowers, T. Isidori, S. Khalil , J. King, G. Krintiras , A. Kropivnitskaya , M. Lazarovits, C. Lindsey, J. Marquez, N. Minafra , M. Murray , M. Nickel, C. Rogan , C. Royon, R. Salvatico , S. Sanders, E. Schmitz, C. Smith , J.D. Tapia Takaki , Q. Wang , Z. Warner, J. Williams , G. Wilson 

Kansas State University, Manhattan, Kansas, USA

S. Duric, A. Ivanov , K. Kaadze , D. Kim, Y. Maravin , T. Mitchell, A. Modak, K. Nam

Lawrence Livermore National Laboratory, Livermore, California, USA

F. Rebassoo, D. Wright

University of Maryland, College Park, Maryland, USA

E. Adams, A. Baden, O. Baron, A. Belloni , S.C. Eno , N.J. Hadley , S. Jabeen , R.G. Kellogg, T. Koeth, A.C. Mignerey, S. Nabili, M. Seidel , A. Skuja , L. Wang, K. Wong 

Massachusetts Institute of Technology, Cambridge, Massachusetts, USA

D. Abercrombie, G. Andreassi, R. Bi, S. Brandt, W. Busza , I.A. Cali, Y. Chen , M. D'Alfonso , J. Eysermans, C. Freer , G. Gomez Ceballos, M. Goncharov, P. Harris, M. Hu, M. Klute , D. Kovalevskyi , J. Krupa, Y.-J. Lee , B. Maier, C. Mironov , C. Paus , D. Rankin , C. Roland , G. Roland, Z. Shi , G.S.F. Stephanos , K. Tatar , J. Wang, Z. Wang , B. Wyslouch 

University of Minnesota, Minneapolis, Minnesota, USA

R.M. Chatterjee, A. Evans , P. Hansen, J. Hiltbrand, Sh. Jain , M. Krohn, Y. Kubota, J. Mans , M. Revering, R. Rusack , R. Saradhy, N. Schroeder , N. Strobbe , M.A. Wadud

University of Nebraska-Lincoln, Lincoln, Nebraska, USA

K. Bloom , M. Bryson, S. Chauhan , D.R. Claes, C. Fangmeier, L. Finco , F. Golf , C. Joo, I. Kravchenko , M. Musich, I. Reed, J.E. Siado, G.R. Snow[†], W. Tabb, F. Yan

State University of New York at Buffalo, Buffalo, New York, USA

G. Agarwal , H. Bandyopadhyay , L. Hay , I. Iashvili , A. Kharchilava, C. McLean , D. Nguyen, J. Pekkanen , S. Rappoccio , A. Williams 

Northeastern University, Boston, Massachusetts, USA

G. Alverson , E. Barberis, Y. Haddad , A. Hortiangtham, J. Li , G. Madigan, B. Marzocchi , D.M. Morse , V. Nguyen, T. Orimoto , A. Parker, L. Skinnari , A. Tishelman-Charny, T. Wamorkar, B. Wang , A. Wisecarver, D. Wood 

Northwestern University, Evanston, Illinois, USA

S. Bhattacharya , J. Bueghly, Z. Chen , A. Gilbert , T. Gunter , K.A. Hahn, Y. Liu, N. Odell, M.H. Schmitt , M. Velasco

University of Notre Dame, Notre Dame, Indiana, USA

R. Band , R. Bucci, A. Das , N. Dev , R. Goldouzian , M. Hildreth, K. Hurtado Anampa , C. Jessop , K. Lannon , J. Lawrence, N. Loukas , D. Lutton, N. Marinelli, I. Mcalister, T. McCauley , F. Meng, K. Mohrman, Y. Musienko⁴⁹, R. Ruchti, P. Siddireddy, A. Townsend, M. Wayne, A. Wightman, M. Wolf , M. Zarucki , L. Zygalas

The Ohio State University, Columbus, Ohio, USA

B. Bylsma, B. Cardwell, L.S. Durkin , B. Francis , C. Hill , M. Nunez Ornelas , K. Wei, B.L. Winer, B.R. Yates 

Princeton University, Princeton, New Jersey, USA

F.M. Addesa , B. Bonham , P. Das , G. Dezoort, P. Elmer , A. Frankenthal , B. Greenberg , N. Haubrich, S. Higginbotham, A. Kalogeropoulos , G. Kopp, S. Kwan , D. Lange, M.T. Lucchini , D. Marlow , K. Mei , I. Ojalvo, J. Olsen , C. Palmer , D. Stickland , C. Tully 

University of Puerto Rico, Mayaguez, Puerto Rico, USA

S. Malik , S. Norberg

Purdue University, West Lafayette, Indiana, USA

A.S. Bakshi, V.E. Barnes , R. Chawla , S. Das , L. Gutay, M. Jones , A.W. Jung , S. Karmarkar, M. Liu, G. Negro, N. Neumeister , G. Paspalaki, C.C. Peng, S. Piperov , A. Purohit, J.F. Schulte , M. Stojanovic¹⁶, J. Thieman , F. Wang , R. Xiao , W. Xie 

Purdue University Northwest, Hammond, Indiana, USA

J. Dolen , N. Parashar

Rice University, Houston, Texas, USA

A. Baty , M. Decaro, S. Dildick , K.M. Ecklund , S. Freed, P. Gardner, F.J.M. Geurts , A. Kumar , W. Li, B.P. Padley , R. Redjimi, W. Shi , A.G. Stahl Leiton , S. Yang , L. Zhang, Y. Zhang 

University of Rochester, Rochester, New York, USA

A. Bodek , P. de Barbaro, R. Demina , J.L. Dulemba , C. Fallon, T. Ferbel , M. Galanti, A. Garcia-Bellido , O. Hindrichs , A. Khukhunaishvili, E. Ranken, R. Taus

Rutgers, The State University of New Jersey, Piscataway, New Jersey, USA

B. Chiarito, J.P. Chou , A. Gandrakota , Y. Gershtein , E. Halkiadakis , A. Hart,

M. Heindl , O. Karacheban²³ , I. Laflotte, A. Lath , R. Montalvo, K. Nash, M. Osherson, S. Salur , S. Schnetzer, S. Somalwar , R. Stone, S.A. Thayil , S. Thomas, H. Wang 

University of Tennessee, Knoxville, Tennessee, USA

H. Acharya, A.G. Delannoy , S. Spanier 

Texas A&M University, College Station, Texas, USA

O. Bouhali⁹⁴ , M. Dalchenko , A. Delgado , R. Eusebi, J. Gilmore, T. Huang, T. Kamon⁹⁵, H. Kim , S. Luo , S. Malhotra, R. Mueller, D. Overton, D. Rathjens , A. Safonov 

Texas Tech University, Lubbock, Texas, USA

N. Akchurin, J. Damgov, V. Hegde, S. Kunori, K. Lamichhane, S.W. Lee , T. Mengke, S. Muthumuni , T. Peltola , I. Volobouev, Z. Wang, A. Whitbeck

Vanderbilt University, Nashville, Tennessee, USA

E. Appelt , S. Greene, A. Gurrola , W. Johns, A. Melo, H. Ni, K. Padeken , F. Romeo , P. Sheldon , S. Tuo, J. Velkovska 

University of Virginia, Charlottesville, Virginia, USA

M.W. Arenton , B. Cox , G. Cummings , J. Hakala , R. Hirosky , M. Joyce , A. Ledovskoy , A. Li, C. Neu , B. Tannenwald , S. White , E. Wolfe 

Wayne State University, Detroit, Michigan, USA

N. Poudyal 

University of Wisconsin - Madison, Madison, WI, Wisconsin, USA

K. Black , T. Bose , J. Buchanan , C. Caillol, S. Dasu , I. De Bruyn , P. Everaerts , F. Fienga , C. Galloni, H. He, M. Herndon , A. Hervé, U. Hussain, A. Lanaro, A. Loeliger, R. Loveless, J. Madhusudanan Sreekala , A. Mallampalli, A. Mohammadi, D. Pinna, A. Savin, V. Shang, V. Sharma , W.H. Smith , D. Teague, S. Trembath-Reichert, W. Vetens 

†: Deceased

1: Also at TU Wien, Wien, Austria

2: Also at Institute of Basic and Applied Sciences, Faculty of Engineering, Arab Academy for Science, Technology and Maritime Transport, Alexandria, Egypt

3: Also at Université Libre de Bruxelles, Bruxelles, Belgium

4: Also at Universidade Estadual de Campinas, Campinas, Brazil

5: Also at Federal University of Rio Grande do Sul, Porto Alegre, Brazil

6: Also at University of Chinese Academy of Sciences, Beijing, China

7: Also at Department of Physics, Tsinghua University, Beijing, China

8: Also at UFMS, Nova Andradina, Brazil

9: Also at Nanjing Normal University Department of Physics, Nanjing, China

10: Now at The University of Iowa, Iowa City, Iowa, USA

11: Also at Institute for Theoretical and Experimental Physics named by A.I. Alikhanov of NRC 'Kurchatov Institute', Moscow, Russia

12: Also at Joint Institute for Nuclear Research, Dubna, Russia

13: Also at Helwan University, Cairo, Egypt

14: Now at Zewail City of Science and Technology, Zewail, Egypt

15: Also at Ain Shams University, Cairo, Egypt

16: Also at Purdue University, West Lafayette, Indiana, USA

17: Also at Université de Haute Alsace, Mulhouse, France

18: Also at Erzincan Binali Yildirim University, Erzincan, Turkey

19: Also at CERN, European Organization for Nuclear Research, Geneva, Switzerland

-
- 20: Also at RWTH Aachen University, III. Physikalisches Institut A, Aachen, Germany
 - 21: Also at University of Hamburg, Hamburg, Germany
 - 22: Also at Isfahan University of Technology, Isfahan, Iran
 - 23: Also at Brandenburg University of Technology, Cottbus, Germany
 - 24: Also at Skobeltsyn Institute of Nuclear Physics, Lomonosov Moscow State University, Moscow, Russia
 - 25: Also at Physics Department, Faculty of Science, Assiut University, Assiut, Egypt
 - 26: Also at Karoly Robert Campus, MATE Institute of Technology, Gyongyos, Hungary
 - 27: Also at Institute of Physics, University of Debrecen, Debrecen, Hungary
 - 28: Also at Institute of Nuclear Research ATOMKI, Debrecen, Hungary
 - 29: Also at MTA-ELTE Lendület CMS Particle and Nuclear Physics Group, Eötvös Loránd University, Budapest, Hungary
 - 30: Also at Wigner Research Centre for Physics, Budapest, Hungary
 - 31: Also at IIT Bhubaneswar, Bhubaneswar, India
 - 32: Also at Institute of Physics, Bhubaneswar, India
 - 33: Also at G.H.G. Khalsa College, Punjab, India
 - 34: Also at Shoolini University, Solan, India
 - 35: Also at University of Hyderabad, Hyderabad, India
 - 36: Also at University of Visva-Bharati, Santiniketan, India
 - 37: Also at Indian Institute of Technology (IIT), Mumbai, India
 - 38: Also at Deutsches Elektronen-Synchrotron, Hamburg, Germany
 - 39: Also at Sharif University of Technology, Tehran, Iran
 - 40: Also at Department of Physics, University of Science and Technology of Mazandaran, Behshahr, Iran
 - 41: Now at INFN Sezione di Bari, Università di Bari, Politecnico di Bari, Bari, Italy
 - 42: Also at Italian National Agency for New Technologies, Energy and Sustainable Economic Development, Bologna, Italy
 - 43: Also at Centro Siciliano di Fisica Nucleare e di Struttura Della Materia, Catania, Italy
 - 44: Also at Università di Napoli 'Federico II', Napoli, Italy
 - 45: Also at Consiglio Nazionale delle Ricerche - Istituto Officina dei Materiali, Perugia, Italy
 - 46: Also at Riga Technical University, Riga, Latvia
 - 47: Also at Consejo Nacional de Ciencia y Tecnología, Mexico City, Mexico
 - 48: Also at IRFU, CEA, Université Paris-Saclay, Gif-sur-Yvette, France
 - 49: Also at Institute for Nuclear Research, Moscow, Russia
 - 50: Now at National Research Nuclear University 'Moscow Engineering Physics Institute' (MEPhI), Moscow, Russia
 - 51: Also at Institute of Nuclear Physics of the Uzbekistan Academy of Sciences, Tashkent, Uzbekistan
 - 52: Also at St. Petersburg Polytechnic University, St. Petersburg, Russia
 - 53: Also at University of Florida, Gainesville, Florida, USA
 - 54: Also at Imperial College, London, United Kingdom
 - 55: Also at Moscow Institute of Physics and Technology, Moscow, Russia
 - 56: Also at P.N. Lebedev Physical Institute, Moscow, Russia
 - 57: Also at California Institute of Technology, Pasadena, California, USA
 - 58: Also at Budker Institute of Nuclear Physics, Novosibirsk, Russia
 - 59: Also at Faculty of Physics, University of Belgrade, Belgrade, Serbia
 - 60: Also at Trincomalee Campus, Eastern University, Sri Lanka, Nilaveli, Sri Lanka
 - 61: Also at INFN Sezione di Pavia, Università di Pavia, Pavia, Italy
 - 62: Also at National and Kapodistrian University of Athens, Athens, Greece

- 63: Also at Ecole Polytechnique Fédérale Lausanne, Lausanne, Switzerland
64: Also at Universität Zürich, Zurich, Switzerland
65: Also at Stefan Meyer Institute for Subatomic Physics, Vienna, Austria
66: Also at Laboratoire d'Annecy-le-Vieux de Physique des Particules, IN2P3-CNRS, Annecy-le-Vieux, France
67: Also at Şırnak University, Şırnak, Turkey
68: Also at Near East University, Research Center of Experimental Health Science, Nicosia, Turkey
69: Also at Konya Technical University, Konya, Turkey
70: Also at Istanbul University - Cerrahpasa, Faculty of Engineering, Istanbul, Turkey
71: Also at Piri Reis University, Istanbul, Turkey
72: Also at Adiyaman University, Adiyaman, Turkey
73: Also at Ozyegin University, Istanbul, Turkey
74: Also at Izmir Institute of Technology, Izmir, Turkey
75: Also at Necmettin Erbakan University, Konya, Turkey
76: Also at Bozok Üniversitesi Rektörlüğü, Yozgat, Turkey
77: Also at Marmara University, Istanbul, Turkey
78: Also at Milli Savunma University, Istanbul, Turkey
79: Also at Kafkas University, Kars, Turkey
80: Also at İstanbul Bilgi University, İstanbul, Turkey
81: Also at Hacettepe University, Ankara, Turkey
82: Also at Rutherford Appleton Laboratory, Didcot, United Kingdom
83: Also at Vrije Universiteit Brussel, Brussel, Belgium
84: Also at School of Physics and Astronomy, University of Southampton, Southampton, United Kingdom
85: Also at IPPP Durham University, Durham, United Kingdom
86: Also at Monash University, Faculty of Science, Clayton, Australia
87: Also at Università di Torino, Torino, Italy
88: Also at Bethel University, St. Paul, Minneapolis, USA
89: Also at Karamanoğlu Mehmetbey University, Karaman, Turkey
90: Also at Bingöl University, Bingöl, Turkey
91: Also at Georgian Technical University, Tbilisi, Georgia
92: Also at Sinop University, Sinop, Turkey
93: Also at Erciyes University, Kayseri, Turkey
94: Also at Texas A&M University at Qatar, Doha, Qatar
95: Also at Kyungpook National University, Daegu, Korea